

1 **Implementation of CCDC to produce the LCMAP Collection 1.0 annual land surface**  
2 **change product**

3 George Z. Xian<sup>1</sup>, Kelcy Smith<sup>2</sup>, Danika Wellington<sup>2</sup>, Josephine Horton<sup>2</sup>, Qiang Zhou<sup>3</sup>,  
4 Congcong Li<sup>3</sup>, Roger Auch<sup>1</sup>, Jesslyn F. Brown<sup>1</sup>, Zhe Zhu<sup>4</sup>, and Ryan R. Reker<sup>2</sup>

5 <sup>1</sup>United States Geological Survey (USGS) Earth Resources Observation and Science (EROS)  
6 Center, Sioux Falls, South Dakota 57198, U.S.A.

7 <sup>2</sup>KBR, Contractor to the USGS EROS Center, Sioux Falls, SD, 57198, U.S.A.

8 <sup>3</sup>ASRC Federal Data Solutions (AFDS), Contractor to the USGS EROS Sioux Falls, SD 57198,  
9 U.S.A.

10 <sup>4</sup>Department of Natural Resources and the Environment, University of Connecticut, Storrs, CT,  
11 U.S.A.

12 Correspondence: George Xian (xian@usgs.gov)

13

14

15

16

17

18

19

20

21

22

23

24

25

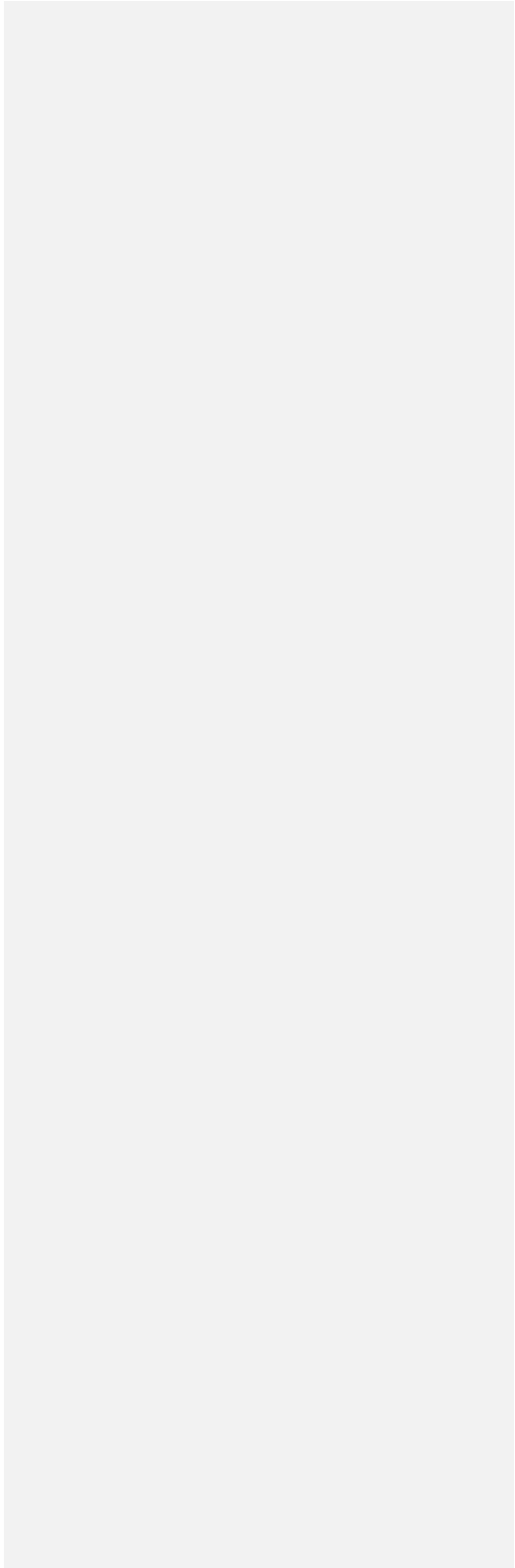
26

27

28

29

30



31 **Abstract**

32 The increasing availability of high-quality remote sensing data and advanced technologies ~~have~~  
33 [has](#) spurred land cover mapping to characterize land change from local to global scales.  
34 However, most land change datasets either span multiple decades at a local scale or cover limited  
35 time over a larger geographic extent. Here, we present a new land cover and land surface change  
36 dataset created by the Land Change Monitoring, Assessment, and Projection (LCMAP) program  
37 over the conterminous United States (CONUS). The LCMAP land cover change dataset consists  
38 of annual land cover and land cover change products over the period 1985-2017 at 30-m  
39 resolution using Landsat and other ancillary data via the Continuous Change Detection and  
40 Classification (CCDC) algorithm. In this paper, we describe our novel approach to implement  
41 the CCDC algorithm to produce the LCMAP product suite composed of five land cover and five  
42 land surface change related products. The LCMAP land cover products were validated using a  
43 collection of ~ 25,000 reference samples collected independently across CONUS. The overall  
44 agreement for all years of the LCMAP primary land cover product reached 82.5%. The LCMAP  
45 products are produced through the LCMAP Information Warehouse and Data Store (IW+DS)  
46 and Shared Mesos Cluster systems that can process, store, and deliver all datasets for public  
47 access. To our knowledge, this is the first set of published 30-m annual land ~~cover and land~~  
48 ~~cover~~ change datasets that [include land cover, land cover change, and spectral change](#) spanning  
49 from the 1980s to the present for the United States. The LCMAP product suite provides useful  
50 information for land resource management and facilitates studies to improve the understanding  
51 of terrestrial ecosystems and the complex dynamics of the Earth system. The LCMAP system  
52 could be implemented to produce global land change products in the future.

53  
54  
55  
56  
57  
58  
59  
60

61 **1 Introduction**

62  
63 ~~The characteristics of land surface fundamentally connect with the functioning of Earth's~~  
64 ~~terrestrial surface.~~ Changes in land cover and land surface are one of the greatest and most  
65 immediate influences on the Earth system, and these changes will continue in association with a  
66 surging human population and growing demand on land resources (Szantoi et al., 2020). Changes  
67 in land cover and ecosystems and their implications for global environmental change and  
68 sustainability are major research challenges for developing strategies to respond to ongoing  
69 global change while meeting development goals (Turner II et al., 2007). Unknowns related to the  
70 spatial extent and degrees of impacts of anthropogenic activities on natural systems and  
71 strategies to respond to ongoing global change hinder efforts to overcome sustainability  
72 challenges (Erb et al., 2017; Reid et al., 2010). An improved understanding of the complex and  
73 dynamic interactions between the various Earth system components, including humans and their  
74 activities, is critical for policymakers and scientists (Foley, 2005; Foley et al., 2011). To fully  
75 understand these processes and monitor these changes, accurate and frequently updated land  
76 cover information is essential for scientific research and to assist decision makers in responding  
77 to the challenges associated with competing land demands and land surface change.

78 The characteristics of land surface fundamentally connect with the functioning of Earth's  
79 terrestrial surface. Satellite observations have been used to observe the Earth's surface and to  
80 characterize land cover and change from local to global scales. Remote sensing data allows us to  
81 obtain information over large areas in a practical and accurate manner. With advanced  
82 technologies and accumulating satellite data, countries and regions have produced multi-spatial  
83 and multi-temporal resolution land cover products (Chen et al., 2015; Gong et al., 2020; Hansen,  
84 2013; Homer et al., 2020; Li et al., 2020). A variety of land change mapping has been carried out  
85 to produce land cover and change products in the United States. Among these efforts are the  
86 widely known National Land Cover Database (NLCD) products. NLCD has provided  
87 comprehensive, general-purpose land cover mapping products at 30-m resolution since 2001 in  
88 the United States, and the products have been published and updated across more than a decade  
89 (Homer et al., 2020). NLCD provides Anderson Level II land cover classification (Anderson,  
90 1976) for the conterminous United States (CONUS) at approximately 2–3-year intervals. Other  
91 national-scale mapping projects focus on specific land cover themes. Among these are the

92 Landscape Fire and Resource Management Planning Tools (LANDFIRE) (Picotte et al., 2019),  
93 which maps vegetation and fuels in support of wildfire management, and the Cropland Data  
94 Layer (Boryan et al., 2011) generated by the National Agricultural Statistics Service (NASS) of  
95 the United States Department of Agriculture (USDA). Due to the need to incorporate data from  
96 neighboring years, as well as extensive post-processing, ancillary dataset dependencies, and  
97 analyst-supported refinement, release dates for both LANDFIRE and NLCD products are  
98 typically several years subsequent to the nominal map year. Other products including national  
99 urban extent change and vegetation phenology data are available (Li et al., 2019; Li et al., 2020).  
100 These projects vary in how land change information is incorporated or expressed across product  
101 releases. Continuous data stacks allow for an increase in input features for land cover  
102 classification. Frequent data also provides the opportunity for near-real time change monitoring  
103 with frequently updated image acquisitions. The availability of land change information has led  
104 to approaches that attempt to monitor surface properties continuously through time (Franklin et  
105 al., 2015; Gong et al., 2019; Hermosilla et al., 2018; Homer et al., 2020; Kennedy et al., 2015; Li  
106 et al., 2020). Such approaches have several advantages over traditional image processing  
107 techniques based on small numbers of images (Bullock et al., 2020; Zhu and Woodcock, 2014b).

108 Leveraging the increasingly massive amount of openly available, analysis-ready data products  
109 into the generation of operational land cover and land change information has been described as  
110 the new paradigm for land cover science (Wulder et al., 2018). The approach, which intended to  
111 use all available medium resolution remotely sensed data from the 1980s to the present, opened a  
112 door for the scientific community to integrate time series information to improve change  
113 detection and land cover characterization in a robust way. Furthermore, change events, when  
114 combined with knowledge of ecology settings or anticipation of a given process post-change, can  
115 accommodate consistent change observations and characterization of land cover. For example,  
116 forest areas that are cleared by wildfire or harvest activities typically transfer to non-forest  
117 herbaceous or shrub vegetation cover, followed by a succession of young tree stages, ultimately  
118 returning to a forest class. Traditional change detection methods using limited observations may  
119 not have identified these changes if data were collected with a starting date prior to the change  
120 and an ending date that occurred after the transitional (non-tree) vegetation returned to tree  
121 cover. Therefore, incorporating change information into the land cover characterization process  
122 allows for insights regarding expected land cover class transitions related to successional

123 processes, and likewise provides a mechanism to identify illogical class transitions and cause or  
124 agent of change (Kennedy et al., 2015; Wulder et al., 2018). The choice of a time series  
125 approach also allows missing data and phenological variations to be handled robustly (Friedl et  
126 al., 2010; Wulder et al., 2018).

127 The Continuous Change Detection (CCD) and Classification (CCDC) algorithm (Zhu and  
128 Woodcock, 2014b; Zhu et al., 2015b) was developed to advance time series change detection by  
129 using all available Landsat data. The CCD algorithm uses robust methodology to identify when  
130 and how the land surface changes through time. The algorithm first estimates a time series model  
131 based on clear observations and then detects outliers by comparing model estimates and Landsat  
132 observations. The algorithm fits harmonic regression models through a Least Absolute Shrinkage  
133 and Selection Operator (LASSO) (Tibshirani, 1996) approach to every pixel over time to  
134 estimate the time series model defined by sine and cosine functions. New Landsat records are  
135 compared to predicted results, and if the observed data deviate beyond a set threshold for all  
136 records within a moving window period, then a model break is produced. The parameters used to  
137 fit the model are used as inputs for the cover classifier for land cover characterization.

138 The original implementation of CCDC was written in the MATLAB programming language and  
139 had been implemented for a regional land cover change assessment in the eastern CONUS (Zhu  
140 and Woodcock, 2014b). The algorithm includes the automation of change detection/classification  
141 and can monitor changes for different land cover types. The implementation of CCDC into a  
142 large geographic extent still encounters several challenges: the availability of Landsat records  
143 and training datasets, the effectiveness of choosing good quality Landsat records, and the  
144 robustness to characterize land cover and change across various land cover types and conditions.  
145 In this paper, we outlined major efforts and challenges in the implementation of CCDC for the  
146 U.S. Geological Survey (USGS) Land Change Monitoring, Assessment, and Projection  
147 (LCMAP) initiative (Brown et al., 2020). LCMAP focuses on using CCD/CCDC with time series  
148 Landsat records and other ancillary information to produce annual land cover and change  
149 products from 1985 to the present for the United States. We focused on how LCMAP employed  
150 every observation in a time series of U.S. Landsat Analysis Ready Data (ARD) (Dwyer et al.,  
151 2018) over a long period starting with the 1980s to determine whether change occurred at any  
152 given point in the observation record. [The CCDC algorithm that was initially developed for](#)

153 [abrupt changes](#) detection on the land surface was modified through lessons learned from the  
154 [prototype test to include both gradual land cover transition and abrupt land change so that the](#)  
155 [algorithm could be used as in an operational setting with the goals of robust, repeatable, and](#)  
156 [geographically consistent results](#) (Brown et al., 2020). The algorithm was further used to classify  
157 the pixel to indicate what land cover type(s) were observed before and after a detected change on  
158 the land surface. [Classification in LCMAP was modified to improve representativeness of](#)  
159 [training data and reduce notable artifacts including misclassification of rare classes and dramatic](#)  
160 [increase in the amount of training data](#). The CCDC algorithm has since been translated into an  
161 open-source library as Python code. The full implementation joined the CCD Python library with  
162 the classification methodology in combination with data delivery/processing services made  
163 available through the LCMAP Information Warehouse and Data Store (IW+DS) [and evolved as](#)  
164 [a national operational monitoring system](#).

165

## 166 **2 Data Sources**

167 The CCDC algorithm utilizes all available Landsat observations including surface reflectance,  
168 brightness temperature, and associated quality data to characterize the spectral responses of  
169 every pixel through harmonic regression model fits. The model fits are then used to categorize  
170 each pixel time series into temporal segments of stable periods and to estimate the dates at which  
171 the spectral time-series data diverge from past responses or patterns. The outcomes of model fits  
172 and other input data are then used for classification. The algorithm requires several input datasets  
173 to perform both change detection and classification.

### 174 **2.1 Landsat observations**

175 U.S. Landsat ARD have been processed to a minimum set of requirements and organized into a  
176 form that can be more directly and easily used for monitoring and assessing landscape change  
177 with minimal additional user effort. Landsat ARD Collection 1 provides consistent radiometric  
178 and geometric Landsat products across Landsat 4-5 Thematic Mapper (TM), Landsat 7 Enhanced  
179 Thematic Mapper Plus (ETM+), and Landsat 8 Operational Land Imager (OLI) / Thermal  
180 Infrared Sensor (TIRS) instruments for use in time series analysis (Dwyer et al., 2018). Landsat  
181 ARD is organized in tiles, which are units of uniform dimension bounded by static corner points  
182 in a defined grid system (Fig. 1). An ARD tile is currently defined as 5,000 x 5,000 30-meter (m)

183 pixels or 150 x 150-kilometer (km). To implement CCDC algorithms to produce LCMAP  
184 Collection 1.0 land change products in CONUS, all available Landsat ARD records of surface  
185 reflectance and brightness temperature from the 1980s to 2017 were required.

## 186 **2.2 Land cover and ancillary datasets**

187 The CCDC algorithm employs every observation in a time series of Landsat data to determine  
188 whether change has occurred at any given time. The algorithm further classifies the time series to  
189 indicate what land cover types were observed before and after a detected change and further to  
190 generate LCMAP annual land cover products (Table 1). The land cover products are produced by  
191 using training data from NLCD in 2001. NLCD provides Anderson Level II (Anderson, 1976)  
192 land cover classification for CONUS and outlying areas (Homer et al., 2020). Spectral index and  
193 change metrics between cloud-corrected Landsat mosaics are used, among other information, to  
194 identify change pixels (Jin et al., 2013). These metrics allow NLCD to incorporate temporal and  
195 spectral trajectory information into both training data selection and final land cover  
196 classification. The NLCD land cover data is used in LCMAP as land cover training data.

197  
198 Ancillary data comprises two main source datasets: the USGS National Elevation Dataset (NED)  
199 (Gesch et al., 2002) 1 arc-second Digital Elevation Models (DEM), and a wetland potential index  
200 (WPI) layer created for NLCD 2011 land cover production (Zhu et al., 2016). The WPI layer is a  
201 ranking (0–8) of wetland likelihood from a comparison of the National Wetland Inventory  
202 (NWI), the U.S. Department of Agriculture Soil Survey Geographic Database (SSURGO) for  
203 hydric soils, and the NLCD 2006 wetlands land cover classes.

204

## 205 **3 Methodology**

206 As part of the operational LCMAP system, the original MATLAB version of the CCDC  
207 algorithm is converted to a format that meets the needs of large-scale land change detection and  
208 change characterization on an annual basis. Python is selected to replace MATLAB to implement  
209 the CCDC algorithm for LCMAP. The CCD component of the CCDC algorithm is converted to  
210 create the Python-based CCD (PyCCD) library. The PyCCD library is a per-pixel algorithm, and  
211 the fundamental outputs are the spectral characterizations (segments) of the input data. There are  
212 several key components in PyCCD. The overall CCD procedures are summarized in Fig. 2.

### 213 3.1 Data filtering and Harmonic modeling

214 The removal of invalid and cloud-contaminated data points is important for deriving model  
215 coefficients that accurately represent the phenology of the surface, and for the correct  
216 identification of model break points. The CCD algorithm uses Landsat ARD PIXELQA values to  
217 mask observations identified as cloud, cloud shadow, fill, or (in some cases) snow derived based  
218 on the Fmask 3.3 algorithm (Zhu et al., 2015a; Zhu and Woodcock, 2012). Additional cirrus and  
219 terrain occlusion bits are provided for Landsat 8 OLI-TIRS ARD that are not available in the  
220 Landsat 4–7 TM/ETM+ quality assessment band. To maintain consistency across the historical  
221 archive, the algorithm does not rely on these Landsat 8-only QA flags to filter out observations.

222 Landsat ARD containing invalid or physically unrealistic data values are removed. For the  
223 surface reflectance bands, the valid data range is between 0 and 10000. Brightness temperature  
224 values, which in the ARD are stored as  $10 \times$  temperature (kelvin), are converted to  $100 \times$  °C and  
225 observations are filtered for values outside the range -9320 and 7070 (-93.2–70.7°C). This  
226 procedure rescales the brightness temperature values into a roughly similar numerical range as  
227 the surface reflectance bands. A multitemporal mask (Tmask) model (Zhu and Woodcock,  
228 2014a) is implemented first to remove additional outliers by using the multitemporal observation  
229 record to identify values that deviate from the overall phenology curve using a specific harmonic  
230 model to perform an initial fit to the phenology. Additional details are provided in the  
231 Supplementary materials S1.

232 The filtered Landsat ARD is further operated to generate the time series fit by harmonic models  
233 whose sinusoidal components are frequency multiples of the base annual frequency. A constant  
234 and linear term characterizes the surface reflectance or brightness temperature offset value and  
235 overall slope, respectively. The full harmonic model is defined as follows:

$$236 \hat{p}(i, t) = c_{0,i} + c_{1,i}t + \sum_{n=1}^3 (a_{n,i} \cos \omega nt + b_{n,i} \sin \omega nt) \quad (1)$$

237 where  $\omega$  is the base annual frequency ( $2\pi/T$ ),  $t$  is the ordinal of the date when January 1 of the  
238 year zero has ordinal 1 (sometimes called Julian date),  $i$  is the  $i$ th Landsat band,  $a_{n,i}$  and  $b_{n,i}$  are  
239 the estimated  $n$ th order harmonic coefficients for the  $i$ th Landsat band,  $c_{0,i}$  and  $c_{1,i}$  are the  
240 estimated intercept and slope coefficients for the  $i$ th Landsat band, and  $\hat{p}(i, t)$  is the predicted  
241 value for the  $i$ th Landsat band at ordinal date  $t$ . Model initialization and certain special-case



242 regression fits such as at the beginning/end of the time series use the simple four-coefficient  
243 model. Outside of these conditions, the selection of coefficient depends on the number of  
244 observations used for the regression. For a full model (eight coefficients), there must be at least  
245 24 observations covered by the regression. The fit parameters returned by PyCCD always  
246 include eight coefficient values including an intercept, with unused coefficients reported as  
247 zeroes.

### 248 **3.2 Regression models and change detection thresholds**

249 The best-fit coefficients for the time series model are calculated using a LASSO regression  
250 model (Tibshirani, 1996). In contrast to Ordinary Least Squares (OLS) that was used in the  
251 original CCDC development, LASSO penalizes the sum of the absolute values of coefficients, in  
252 some cases forcing a subset of the coefficients to zero. Together with the explicit limits enforced  
253 on the number of coefficients, this reduces instances of overfitting, including in cases when  
254 observations are too sparse or unevenly distributed in time to constrain the model to real  
255 phenological features. To detect change, the LASSO model checks CCD model breaks with  
256 respect to its last determined best-fit harmonic model.

257 To correctly detect change, the algorithm distinguishes between a substantive deviation from  
258 model prediction and deviations that result from variability inherent in the data (due to  
259 incomplete atmospheric removal and/or other sources of natural variation) to detect change. The  
260 algorithm calculates two parameters related to dispersion, or scatter, to estimate the variability of  
261 data for each spectral band. The first one is a comparison root-mean-square-error (RMSE) that is  
262 the RMSE of the 24 observations covered by the model which are closest in day of year to the  
263 last observation in the “peek window,” or over all observations covered by the model if there are  
264 fewer than 24. This value is recalculated at each step of the time series. The second parameter  
265 (*var*) is used to measure the overall variability of the data values and is defined as the median of  
266 the absolute value of the differences between each observation and the *i*th successive  
267 observation, where *i* is the smallest value such that the majority of these observation pairs are  
268 separated by greater than 30 days, if possible (otherwise, *i*=1). The *var* is computed once at the  
269 beginning of the standard procedure, using all non-masked observations in the time series.

270 Observations not yet incorporated into the model are evaluated as a group of no fewer than the  
271 *PEEK\_SIZE* parameter value; this is the “peek window,” which “slides” along the time series

272 one observation at a time. Each iteration, a value is calculated for each individual observation  
273 within the peek window, as follows:

$$mag_n = \sum_{i \in D} \left( \frac{resid_{n,i}}{\max(var_i, RMSE_i)} \right)^2 \quad (2)$$

274 where,  $resid_{n,i}$  is the residual relative to the LASSO models for each band  $i$ , for each  
275 observation  $n$  within the  $PEEK\_SIZE$  window,  $var_i$  and  $RMSE_i$  are the parameters of dispersion  
276 as described above, for each band  $i$ . This summation is carried out for all bands  $i$  in the set of  
277  $DETECTION\_BANDS$  ( $D$ ). This produces a scalar magnitude, representing the deviation from  
278 model prediction across these bands, for each observation. The detection of a model break  
279 requires this value to be above the  $CHANGE\_THRESHOLD$  value for all observations in the  
280 window. This is separate from the value that is reported as a per-band magnitude when a change  
281 is detected in the time series. Change detection sensitivity depends on the value of change  
282 threshold. The  $CHANGE\_THRESHOLD$  is determined in Eqs. S2 and S3 in the Supplementary.  
283 If  $mag_n < CHANGE\_THRESHOLD$  for any  $n$  in the  $Peek\_Size$  window, then add the most  
284 recent observation to the segment by shifting the  $Peek\_Size$  window one observation forward in  
285 the time series. If  $mag_n > CHANGE\_THRESHOLD$  for all  $n$  in the  $Peek\_Size$  window, this is  
286 considered a spectral break.

### 287 3.3 Permanent snow and insufficient clear observation procedures

288 The permanent snow procedure indicates that too few clear (less than 25% of total observations)  
289 or water observations, which are identified from the QA band, exist to robustly detect change,  
290 and a large fraction of observations are snow. The algorithm will return at most one segment that  
291 fits through the entire time series and provide the filtered observations number at least twelve.  
292 The model will, under the default settings, fit only four coefficients (i.e., characterizing the  
293 reflectance and brightness temperature bands using only a simple harmonic with no higher  
294 frequency terms). Unlike other procedures, snow pixels are not filtered out and are fit as part of  
295 the annual pattern. This avoids overfitting the model to a seasonally sparse observation record.  
296 Similarly, for the insufficient clear observations determined by the QA band, the model will  
297 perform a LASSO regression fit for the entire time series using four coefficients. The model  
298 coefficients and RMSE from this regression are recorded. Additional parameters including the  
299 start, end, and observation count are also saved. Further, the change Boolean value is set to 0,

300 and the break day is recorded as the last observation date. The magnitude of change as zero for  
301 each band is also saved.

### 302 **3.4 Land cover classification**

303 The CCDC algorithm characterizes the land cover component of a pixel at any point using the  
304 LCMAP time series model approach from the Landsat 4–8 records. The classification of CCDC  
305 is accomplished for every pixel based on data from the time series models (e.g., model  
306 coefficients). Land cover classifications are generated on an annual basis, using July 1st as a  
307 representative date. A list of land cover classes and descriptions is provided in Table 1. [Fig.3](#)  
308 [illustrates an overall classification approach.](#)

#### 309 **3.4.1 Classification algorithm**

310 We chose eXtreme Gradient Boosting (XGBoost) (Chen and Guestrin, 2016) as the classification  
311 method. XGBoost is a scalable implementation of gradient tree boosting, which is a supervised  
312 learning method that can be used to develop a classification model when provided with an  
313 appropriate training dataset. Generally, for a given dataset, a tree ensemble model uses additive  
314 functions, which correspond to independent tree structures, to predict the land cover. The  
315 predictions from all trees are also normalized to the final class probabilities using the softmax  
316 function. The algorithm can handle sparse data and theoretically justify weighted quantile sketch  
317 for approximate learning. The resultant trained model can be applied to a larger dataset to  
318 generate predictions and probability scores which are the basis for LCMAP primary and  
319 secondary land cover types. The primary and secondary land cover confidence values are  
320 calculated from these scores.

#### 321 **3.4.2 Training dataset**

322 The training data used in XGBoost for the LCMAP Collection 1.0 land cover products is from  
323 the USGS NLCD 2001 land cover product (Homer et al., 2020). To meet the LCMAP land cover  
324 legend, the NLCD data is first cross-walked to LCMAP classes, as shown in Fig.43 and Table 2.  
325 [The use of NLCD data that was cross-walked to the LCMAP land cover legend as the training](#)  
326 [data will reduce uncertainties and improve the ~~consistence~~consistency of annual land cover](#)  
327 [change. For example, grass and shrub have different ecological functions. Their spectral](#)  
328 [signatures are distinct in some ecological regions but are very close in ~~some regions~~others.](#)

329 [especially in the western ecoregions of the conterminous United States \(Underwood et al., 2007;](#)  
330 [Xian et al., 2013\)](#). [Grass and shrub usually grow close together, making it difficult to separate](#)  
331 [them in thematic land cover. By eCombining these two cover classes together can reduce](#)  
332 [uncertainties potentially caused by lack of spectral ~~distinct of~~ distinction in Landsat observations.](#)  
333 [Furthermore, t](#)The extent of each land cover in the cross-walked NLCD layer is eroded by one  
334 pixel. This step aims to reduce potential noise in the classifier by removing pixels that may be  
335 heavily mixed with different cover types, or whose land cover label may be less reliable. It also  
336 removes the narrow linear low-intensity developed pixels corresponding to road networks, which  
337 were found to have registration issues with Landsat ARD in some areas.

338

### 339 **3.4.3 Ancillary data**

340 Ancillary data used in the classification contains two main datasets: the DEM and the WPI layer.  
341 Three DEM derivative datasets are implemented as geographic references for land cover  
342 classification as ancillary data including topographic slope, aspect, and position index. The WPI  
343 is highly related to wetland distribution and has a potential to improve wetland classification in  
344 LCMAP.

### 345 **3.4.4 Classification procedures**

346 For each pixel, CCD segment data for the segment that includes the July 1st, 2001 date is used  
347 with training data to create classification models (Zhou et al., 2020; Zhu et al., 2016). [Data](#)  
348 [generated from the CCD models are used to make the land cover classification because different](#)  
349 [land cover classes can have different shapes for the estimated time series models. The](#)  
350 [coefficients of the CCD models including the overall mean and model coefficients except](#)  
351 [intercepts can be used to estimate the intra-annual changes caused by phenology and sun angle](#)  
352 [differences for the  \$i\$ th Landsat band. The information obtained from the time series model is](#)  
353 [useful for land cover classification.](#) The CCD model data used with training data include the  
354 model coefficients (except the intercepts) generated from surface reflectance and brightness  
355 temperature bands, the model RMSE value for each band, and an average intercept value that is  
356 calculated from average annual reflectance values for each band for the July 1, 2001 year. The  
357 model training procedure is conducted at the tile level, using random samples drawn from the  
358 targeted tile as well as the eight surrounding tiles to avoid not having enough training samples of

359 rare land cover types in the targeted tile. Cross-walked and eroded NLCD data are used for  
360 classification labels, while the CCD model outputs and ancillary data are provided as  
361 independent variables. Based on training data testing using different sample sizes, a target  
362 sample size of 20 million pixels from the extent of 3x3 ARD tiles is chosen, requiring  
363 approximately proportional representation of classes with the added constraint that no class be  
364 represented by fewer than 600,000 or more than 8 million samples. If there are fewer than  
365 600,000 samples available for a class, then all of the available samples are used without any  
366 oversampling. The XGBoost hyperparameters are selected as: maximum tree depth 8, fast  
367 histogram optimized approximate greedy algorithm for tree method, multiclass logloss for  
368 evaluation metric, and maximum number of rounds 500.

369 After the classification models in a given tile are trained, predictions are generated for each July  
370 1st date that has an associated CCD segment (Fig. 54). The prediction information is supplied to  
371 the production step for the creation of land cover. The process is repeated for each tile for the  
372 entire CONUS ARD extent.

### 373 **3.5 Validation data**

374 The LCMAP land cover product is validated using an independent reference dataset. The  
375 reference data, which consists of 24,971 30 m x 30 m pixels selected via a simple random  
376 sampling method over CONUS, is collected from these sample plots between 1985 and 2017.  
377 The TimeSync tool is used to efficiently display Landsat data for interpretation and to record  
378 these interpretations into a database (Cohen et al., 2010; Pengra et al., 2020b; Stehman et al.,  
379 2021). TimeSync displays the input Landsat images in two basic ways: by annual time-series  
380 images and by pixel values plotted through time. For the image display, single 255 x 255-pixel  
381 subsets of Landsat images in the growing season are displayed in sequence from 1984 to 2018.  
382 Trained interpreters have access to all available images in each year to collect attributes in three  
383 basic categories: 1) land use, 2) land cover, and 3) change processes. Additional attribute details  
384 for the change processes, such as clear-cut and thinning associated with harvest events, are also  
385 collected. The interpreters manually label these attributes using Landsat 5, 7, and 8 imagery,  
386 high-resolution aerial photography, and other ancillary datasets (Cohen et al., 2010; Pengra et al.,  
387 2020b). Interpreters also use ancillary data to support interpretation of Landsat and high-  
388 resolution imagery, although Landsat data takes the highest weight of evidence. Recording the

389 full set of attributes in land use, land cover, and land change categories provides sufficient  
390 information to meet the needs of LCMAP as well as other potential users. Quality assurance and  
391 quality control (QA/QC) processes are also implemented to ensure the quality and consistency of  
392 the reference data among interpreters and over the time span of data collection (Pengra et al.,  
393 2020b). ~~All~~Each reference samples are is each interpreted by a trained interpreter and about 60%  
394 of these pixels are interpreted independently by a second analyst. Much of the QA/QC process  
395 relies on comparing the interpretations at these duplicated sample pixels. Duplicated sample  
396 pixels that have interpreter disagreement are evaluated in the QA/QC process, ~~that~~  
397 ~~focuses~~focusing on identifying issues with specific classes or interpreters, flagging sample pixels  
398 for further review and possible editing, and providing ongoing training and feedback to  
399 interpreters throughout the collection process. QA/QC related reviews are also completed on  
400 sample pixels that show interpretation data such as uncommon and/or illogical land use and land  
401 cover combinations, multi-year disturbance processes, rare classes, or other opportunistically  
402 identified situations. Interpreted attributes of sample pixels are edited, if necessary, to create the  
403 final attribute assignments for the reference data. These final attributes are then cross-walked to  
404 a single LCMAP land cover class label~~The collected samples are then cross-walked to the~~  
405 ~~appropriate LCMAP land cover class~~, providing a single land cover reference label for each year  
406 of the time series for each sample pixel.

407 The validation analysis protocols focus on estimating the confusion matrix and overall, user's,  
408 and producer's accuracy by comparing the reference data and product data labels. Overall  
409 accuracy and producer's accuracy as well as standard errors are produced using post stratified  
410 estimators (Card, 1982; Stehman, 2013). For accuracy estimates that are produced by combining  
411 multiple years of data, the sampling design is treated as a one-stage cluster sample where each  
412 pixel represents a cluster and each year of observation is the secondary sampling unit using  
413 cluster sampling standard error formulas (Pengra et al., 2020b; Stehman et al., 2021). The  
414 validation is only performed for primary land cover and change products, not for other LCMAP  
415 science products (Supplementary Section 4).

### 416 **3.6 Information warehouse and data store**

417 ~~The~~ LCMAP adopts an information warehouse and data store (IW+DS) system that can expand  
418 storage solutions along with data access and discovery services running on the EROS Shared

419 Mesos Cluster. The system provides different storage solutions to allow for flexibility in  
420 choosing what best fits a dataset's characteristics and currently comprises Apache Cassandra  
421 (<https://cassandra.apache.org/>) and Ceph (<https://ceph.io/>) object storage. The services provide  
422 data ingest, retrieval, discovery, metadata, processing, and other functionalities. LCMAP  
423 maintains a copy of Landsat Collection 1 ARD and other similarly tiled ancillary datasets that  
424 are spatially subset within the IW+DS to allow efficient retrieval and to enable large-scale  
425 CCDC processing and other algorithmic work. The ingest process is designed to avoid bringing  
426 in ARD tile observations that are already present within the IW+DS, to keep the input consistent  
427 with any prior usage while allowing CCDC to bring in new observations as they are available.  
428 Algorithmic results, products, and other intermediate data are kept on the Ceph object store  
429 arranged using a prefix structure to label the identity of the data, with the actual object names  
430 incorporating spatial concepts such as tile and chip that is a small subset of a tile and contains  
431 100 by 100 30\_m pixels.

432

## 433 **4 Results and Discussion**

434

435 The LCMAP primary land cover and change products were evaluated to outline annual land  
436 cover change from 1985 to 2017 in the conterminous Unites States.

### 437 **4.1 Collection 1.0 primary land cover distribution and change**

438 The CONUS primary land cover mapping result and the primary confidence in 2010 are shown  
439 in Fig. [6.5a](#) and b, respectively. The land cover map illustrates distributions of different land  
440 cover types across CONUS. The primary confidence is above 90% for most land cover classes,  
441 suggesting that the classification models were created with high confidence for land cover  
442 mapping for most classes in most regions. Some vegetation transition (~~dark~~-green in Fig. [6.5b](#))  
443 occurs mainly in the southeast region suggesting gradual tree recovery from disturbances  
444 associated with tree harvesting. Fig. [6.5c](#) and d display numbers of land cover changes and  
445 spectral changes detected by the CCDC model between 1985 and 2017. The number of land  
446 cover changes represents how many times land cover has changed from one type to another for a  
447 specific pixel. However, the number of spectral changes denotes how many times the model has  
448 detected spectral changes in a CCD time series model where spectral observations have diverged

449 from the model predictions. These changes could relate to a change in thematic land cover or  
450 might represent more subtle conditional surface changes. The southeast region shows more  
451 frequent land cover changes in the 33 years (Fig. 6.5c). The western part of CONUS, however,  
452 contains more spectral changes than in the east (Fig. 6d). [The NLCD land change estimates also](#)  
453 [show the similar change patterns between 2001 and 2016 \(Homer et al., 2020\).](#) The  
454 different spatial patterns in the total number of land cover changes (Fig. 6.5c) and detected  
455 spectral changes (Fig. 6.5d) suggest that not all changes lead to land cover change (e.g., drought  
456 and precipitation-related changes in vegetation or grassland fire). The large numbers of spectral  
457 change were mainly detected in the southern grassland area.

458 Fig. 7.6 shows the temporal changes of areas for eight land cover classes from 1985 to 2017.  
459 Among all classes, grass/shrub, tree cover, and cropland were dominant land cover types,  
460 followed by wetland, water, developed, barren, and snow/ice. The land cover and change  
461 datasets show that developed land has a consistent increasing trend with an 8.4% increase while  
462 barren increased 9.1% between 1985 and 2017. Overall, the developed and barren areas  
463 increased  $2.58 \times 10^4 \text{ km}^2$  and  $8.56 \times 10^3 \text{ km}^2$ , respectively. Other land cover categories do not have  
464 such increasing patterns. As for water, although fluctuating, it had a generally increasing trend.  
465 The area of wetland had a rapid decrease before 2000, following a relatively steady though  
466 fluctuating trend. Net wetland extent declined about 0.4% from 1985 to 2017. The grass/shrub  
467 and tree cover classes both experienced consistent increasing trends before 2008 and 1995,  
468 [respectively](#), with areas reaching about  $2.85 \times 10^6 \text{ km}^2$  for grass/shrub and  $2.14 \times 10^6 \text{ km}^2$  for tree  
469 in these two years. These two land covers gradually decreased since then. Tree cover declines  
470 after 1996, showing a decreasing rate of 2.8% between 1985 and 2017. The cropland decreased  
471 from 1985 to 2008 and quickly increased after that. By 2017, the area of cropland reached a  
472 similar level of cropland area in 1988. Furthermore, most land cover changes are located in the  
473 southeast region where many pixels change more than one time. The changes detected by the  
474 CCD model suggest that landscape in the Midwest and west are more dynamic than in the east.  
475 Many areas experience multiple disturbances although most of these changes do not result in  
476 land cover transition.

477 The south ARD tile outlined in Fig. 6.5(a) covers the northern Dallas region, and the spatial  
478 patterns of land cover and change are shown in more detail in Fig. 8.7. The land cover



479 distributions in the region show that urban land expands considerably from 1985 (Fig. 87a), to  
480 1990 (Fig. 78b), and to 2016 (Fig. 87c). The land conversion was primarily from cropland and  
481 grass/shrub to developed land. Lake Ray Roberts was created in the late 1980s and captured in  
482 the land cover map (Fig. 87b&c). The lake and urban conversion are also visible in the change  
483 count from 1985 to 2016 (Fig. 87g), which mainly show as blue, suggesting a one-time  
484 conversion. On the other hand, there is almost no change in the urban center (Fig. 87g). Fig. 78  
485 (d-f) shows high classification confidence at the urban center, water, grass/shrub, and tree cover  
486 areas, whereas cropland has relatively low confidence, indicating frequent management activities  
487 over croplands in the regions. The total pixels of different change numbers suggest that one to  
488 two change times are dominant, although some pixels change more than three times (Fig. 87h).  
489 The land cover distributions in 1985, 1990, and 2017 show an increase in developed land and  
490 decreases in cropland and grass/shrub (Fig. 87i).

491 The spatial patterns of land cover and change in the north ARD tile displayed in Fig. 65(a) in  
492 northern Wyoming are shown in Fig. 98. The tile covers most of Yellowstone National Park, in  
493 which tree, grass/shrub, and water are three dominant land cover types. Land cover in 1985,  
494 1990, and 2016 (Fig. 98a-c) changed from tree to grass/shrub and back to tree cover. The  
495 primary land cover confidence layers exhibit changes as decreasing vegetation from tree to  
496 grass/shrub and increasing vegetation from grass/shrub to tree (Fig. 98d-f). For those trees and  
497 water bodies that did not experience any disturbances, their magnitudes of confidence are  
498 relatively large. The change map suggests that most forest lands experienced at least one change  
499 and some areas changed multiple times (Fig. 98g). Most changes in forest lands were related to  
500 wildland fires that occurred in the region. In 1988, 50 fires burned a mosaic covering nearly 3213  
501 km<sup>2</sup> in Yellowstone as a result of extremely warm, dry, and windy weather (NPS, 2021). Trees  
502 regrew in some of the burn areas and these changes could occur more than once as shown in the  
503 change map that indicates at least two changes in these areas. The total pixels of different change  
504 frequencies suggest that one to two changes were dominant and very few pixels changed more  
505 than three times (Fig. 98h). The land cover distributions in 1985, 1990, and 2017 had increases in  
506 grass/shrub after 1985 and reductions in tree cover after that (Fig. 98i).

#### 507 **4.2 Validation of land cover product**

508 The overall accuracy between the annual reference land cover label and the LCMAP annual land  
509 cover products was calculated as 82.5% ( $\pm 0.22\%$ , standard error) when summarized for all years.  
510 Overall accuracy across the time series (1985-2017) varied within about 1.5% annually, ranging  
511 from a high of 83% in the late 1990s to about 82% in the late 2010s (Fig. 109). Per class  
512 accuracies across CONUS ranged between 43% and 96% for user's accuracy (Table 3), with  
513 water showing the highest accuracy (96%  $\pm 0.5\%$  user's accuracy and 93%  $\pm 0.7\%$  producer's  
514 accuracy). Cropland has about 93% ( $\pm 0.3\%$ ) producer's accuracy and 70% ( $\pm 0.6\%$ ) user's  
515 accuracy. The lowest accuracies are observed for barren and wetland. The per class per year  
516 agreements show the accuracies vary slightly for each class in each year (Table 4). The  
517 variations of annual overall accuracy are within a range of about 1.5% across the time series. The  
518 slightly decline in annual overall accuracy suggests that year-to-year trends may be a result of a  
519 complex interplay of temporal biases in the LCMAP algorithm, Landsat data quality and  
520 quantity, the model break detection accuracy of the LCMAP CCD, and errors in the training data  
521 used for the classification. For example, the change detection portion of the algorithm is known  
522 to be conservative in identifying land cover change. The CCD model assumes that the spectral  
523 variations of the land surface through time can be characterized with annual harmonic models  
524 and can be separated into discrete periods of time. Therefore, the model performs better when the  
525 short-term spectral variability of the land surface is low, and the changes can be sought after  
526 have a large spectral response, and the observational data density is high. Over time, the actual  
527 land cover may evolve away from the phenology represented by spectral models that may have  
528 missed one or more spectral breaks, which will impact accuracy especially when the land cover  
529 changes are persistent rather than cyclic, such as with an expanding urban footprint. Annual  
530 accuracy of Developed showed an upward trend in user's accuracy (UA) and a downward trend  
531 in producer's accuracy (PA) over time (Stehman et al., 2021). The increasing availability of  
532 high-resolution data used by the interpreters may have increased the likelihood of identifying  
533 features characteristic of Developed land that could not be identified earlier in the time series,  
534 thus leading to an increase in the proportion of Developed area of Developed-estimated from the  
535 sample. Consequently, the increasing sensitivity of the reference interpretation to landscape  
536 features may account for the difference between the mapping and the reference data over time.  
537 Lower data density toward the beginning and end of the time series may decrease accuracy.

538 [which when combined with other factors, can contribute to the annual land cover overall](#)  
539 [accuracy across all years.](#)

#### 540 **4.3 Significance of the product**

541 One of the biggest advances of LCMAP relative to conventional methods available to date is its  
542 approach of generating annual land change products by using the entire Landsat archive at a  
543 large geographic scale. Landsat ARD, which is the foundation for LCMAP, is effective and  
544 straightforward for tracking and characterizing the historical land changes at a pixel level over  
545 decades. Compared to conventional methods, detecting changes using all available observations  
546 enables us to date these changes as they occur. After change is detected, temporally consistent  
547 land cover products rather than stochastic changes in labels can be produced at annual intervals  
548 by conducting classification from CCD model segmented contributions

549 The LCMAP product suite includes five land cover change and five land surface change science  
550 products. It represents a new paradigm that consistently and continuously provides a large  
551 volume of land change information for land change monitoring, land resource management, and  
552 scientific research. In addition to primary and secondary land cover before and after changes,  
553 change segments containing spectral change time and magnitude are provided to explore the  
554 changes in land condition and could meet various user communities' needs. The LCMAP  
555 products can improve our understanding of causes, rates, and consequences of the land surface  
556 changes (Rover et al. 2020) such as forest changes caused by wildfire and insect outbreaks.

557 By implementing the CCDC algorithm through a system engineering approach, LCMAP  
558 provides a fully automated framework for land change monitoring. The framework can also be  
559 updated to include the latest Landsat records so that it can be used for operational continuous  
560 monitoring in a large geographic extent (Brown et al. 2020). Therefore, when new observations  
561 become available, the framework can provide timely and consistent land cover characteristics to  
562 the public.

#### 563 **4.4 Limitations and challenges**

564 Although LCMAP Collection 1.0 products have been proven to be successful in detecting  
565 various land surface changes to support research applications related to environment and ecology  
566 conditions, limitations and challenges exist. Utilizing Landsat ARD data as input provided

567 consistent time series Landsat imagery with high level geometric and radiometric quality for  
568 implementing the CCDC method. Nevertheless, the densities of Landsat observation records  
569 varied greatly across space and time due to spatial differences in Landsat scene overlap and  
570 temporal coverage, as well as regional differences in contamination by clouds, cloud shadows,  
571 and snow. The change detection accuracies of CCD models were highly influenced by the  
572 temporal frequency of available observations. Zhou et al. (2019) found that using harmonized  
573 Landsat-8 and Sentinel-2 (HLS) data increased the temporal frequency of the data and thus  
574 enhanced the ability to model seasonal variation and derived better change detection results than  
575 using Landsat data alone. Integrating multi-mission data could provide the opportunity to  
576 enhance change detection, especially for the land cover types that are highly dynamic or in  
577 frequently cloudy/snowy areas.

578 Providing only eight general land cover classes and their changes in LCMAP Collection 1.0  
579 products limits the usage of the product in some applications that need a higher level of thematic  
580 land cover detail. For example, shrub and grass are two major vegetation types and have  
581 different ecological functions, but they are not delineated separately in LCMAP Collection 1.0  
582 products. Lack of measurement of grassland-shrub transition constrains the study of shrub  
583 encroachment, which is a symptom of land degradation. However, NLCD 2001 level I land  
584 cover product had different mapping accuracies for different land cover types in different  
585 ecological regions (Wickham et al., 2010). For example, the grass mapping accuracies were  
586 higher in the eastern regions than they were in the most of western mapping regions. The  
587 accuracies of shrub cover had the similar variation patterns across the CONUS. These  
588 accuracy variations suggest uncertainties of the products, especially in the most of western  
589 regions where grass and shrub are more difficult to be separated. The use of NLCD 2001 product  
590 by eCombining grass and shrub together from the NLCD 2001 product reduced uncertainties  
591 introduced by the two individual components and made the accuracy of the grass/shrub product  
592 in of LCMAP product relatively high and consistent across CONUS (Stehman et al., 2021).  
593 NLCD has established new efforts to improve mapping accuracies by adding  
594 innovated innovative approaches for land cover classification and introducing continuous  
595 rangeland products in the west of western CONUS for NLCD thematic land cover products since  
596 2001 (Homer et al., 2020). The use of new NLCD products as the training data will support  
597 LCMAP to produce more land cover types including separating grass and shrub in the future.

598 Adopting NLCD ~~2001~~ [land cover product](#) as the training data source efficiently provided  
599 abundant training samples to deliver land cover product with high classification accuracy. ~~To~~  
600 ~~select~~ [Selecting a sufficient size of training samples is important for CCDC models to obtain](#)  
601 [accurate classification. Previous land cover post-classification analysis suggested that the overall](#)  
602 [classification accuracy increased when the training samples increased \(Gong et al., 2020\). The](#)  
603 [recent global land cover classification also suggested that the appropriate training sample size for](#)  
604 [a mapping extent of three 158 km x 158 km tiles should be larger than 60,000 \(Zhang et al.,](#)  
605 [2021\). For the LCMAP land cover classification, a much larger ~~size~~-training size was utilized to](#)  
606 [ensure that these training samples could represent landscape features in the classification tiles.](#)  
607 However, these training data were randomly selected from the NLCD land cover product,  
608 suggesting errors could potentially be carried over to the training samples due to potential errors  
609 in the training source. Besides uncertainties in training data, some obvious challenges such as  
610 class definitional differences between pasture/hay and grassland between NLCD and LCMAP  
611 could potentially be carried over to the LCMAP land cover product. ~~Implementing~~-[Improving](#)  
612 training data by reducing uncertainties and potential errors in a more consistent and accurate way  
613 is critical to strengthen land cover classification and to improve the scientific quality of LCMAP  
614 products in the future.

615 There are apparent shifts in some land cover types, especially in snow/ice and barren (Fig. [7.6](#)),  
616 and a decline in overall agreement (Fig. [10.9](#)) in 2017, the last year of the Collection 1.0 product.  
617 The last year's product usually is provisional because limited Landsat observations are available  
618 at the end of a time series. The CCDC requires at least 24 clear observations to create full models  
619 for change detection and classification. Without sufficient clear observations, the algorithm  
620 could not produce model break accurately. Therefore, in the last year of a time series, the rule-  
621 based assignment is implemented to label land cover for these pixels that do not have enough  
622 observations to build a time series model. Both primary and secondary land cover classes are  
623 assigned from the last identified primary and secondary classes.

624

## 625 **5 Data Availability**

626 The LCMAP products generated in this paper are available at <https://earthexplorer.usgs.gov/>  
627 (LCMAP, 2021). All LCMAP land change products are mosaiced for the conterminous United

628 States in the GeoTIFF format. Find exact data as described here at  
629 <https://doi.org/10.5066/P9W1TO6E>. The reference dataset used for the product validation is also  
630 available at <https://www.sciencebase.gov/catalog/item/5e57e965e4b01d50924a93f6>  
631 or <https://doi.org/10.5066/P98EC5XR> (Pengra et al., 2020a).

632

## 633 **6 Conclusions**

634 The continuous Landsat observations spanning from the 1980s to the present, new generations of  
635 change detection and classification models, and systems capable of processing large volume data  
636 are offering unprecedented opportunities to characterize land cover and detect land surface  
637 change consistently and accurately. Additionally, the collection of reference data used to validate  
638 land cover products provides validation result for each land cover category annually. To capture  
639 the variability of landscape condition and its responses to different disturbances, land cover and  
640 land surface change datasets need to be produced over a large geographic scale. ~~The~~ LCMAP has  
641 produced a suite of land change product ~~in~~at 30-m resolution including the reference dataset in  
642 the United States. In that context, LCMAP was developed to generate an essential dataset to  
643 meet broad scientific research and resource management needs. Using the CCDC algorithm and  
644 Landsat ARD to determine whether change has occurred at any given point in the observation  
645 record, LCMAP produced annual land cover and change datasets for the conterminous United  
646 States in a robust manner. These new datasets and the novel production systems will allow for  
647 new generation of research and applications in connecting time series remote sensing  
648 observations with land surface change at a much finer scale than previously possible.

649

650 **Supplement.** The supplement related to this article is attached.

651

## 652 **Author contributions.**

653 KS conducted PyCCD programming for CCD/CCDC models. ZZ developed the original  
654 MATLAB version of CCD/CCDC programs. JH participated in reference data collection. DW  
655 and QZ assisted in data integration tasks. GX analysed the data and wrote the manuscript with  
656 contributions from all co-authors.

657

658 **Completing interests.** The authors declare that they have no conflict of interest.

659

660 **Acknowledgements.**

661 Any use of trade, firm, or product names is for descriptive purposes only and does not imply  
662 endorsement by the U.S. Government. Qiang Zhou and Congcong Li's work were performed  
663 under Work performed under USGS contract 140G0119C0001.

664

665

666

## References

- Anderson, J. R., Hardy, E.E., Roach, J.T., and Witmer, R.E.: A land use and land cover classification system for use with remote sensor data, Geological Survey Professional Paper, 964, 1-28, 1976.
- Boryan, C., Yang, Z., Mueller, R., and Craig, M.: Monitoring US agriculture: the US department of agriculture, national agricultural statistics service, cropland data layer program, Geocarto International, 26, 341-358, 2011.
- Brown, J. F., Tollerud, H. J., Barber, C. P., Zhou, Q., Dwyer, J. L., Vogelmann, J. E., Loveland, T. R., Woodcock, C. E., Stehman, S. V., Zhu, Z., Pengra, B. W., Smith, K., Horton, J. A., Xian, G., Auch, R. F., Sohl, T. L., Saylor, K. L., Gallant, A. L., Zelenak, D., Reker, R. R., and Rover, J.: Lessons learned implementing an operational continuous United States national land change monitoring capability: The Land Change Monitoring, Assessment, and Projection (LCMAP) approach, Remote Sensing of Environment, 238, 111356, 2020.
- Bullock, E. L., Woodcock, C. E., and Holden, C. E.: Improved change monitoring using an ensemble of time series algorithms, Remote Sensing of Environment, 238, 2020.
- Chen, J., Liao, A., Cao, X., Chen, L., Chen, Z., He, C., Han, G., Peng, S., Lu, M., and Zhang, W.: Global land cover mapping at 30 m resolution: A POK-based operational approach, ISPRS journal of photogrammetry and remote sensing : official publication of the International Society for Photogrammetry and Remote Sensing, 103, 7-27, 2015.

Chen, T. and Guestrin, C.: XGBoost, Proceedings of the 22nd ACM SIGKDD International Conference on Knowledge Discovery and Data Mining, 785-794, 2016.

Cohen, W. B., Yang, Z., and Kennedy, R.: Detecting trends in forest disturbance and recovery using yearly Landsat time series: 2. TimeSync — Tools for calibration and validation, *Remote Sensing of Environment*, 114, 2911-2924, 2010.

Dwyer, J. L., Roy, D. P., Sauer, B., Jenkerson, C. B., Zhang, H. K., and Lymburner, L.: Analysis Ready Data: Enabling Analysis of the Landsat Archive, *Remote Sensing*, 10, 1363, 2018.

Erb, K. H., Luysaert, S., Meyfroidt, P., Pongratz, J., Don, A., Kloster, S., Kuemmerle, T., Fetzel, T., Fuchs, R., Herold, M., Haberl, H., Jones, C. D., Marin-Spiotta, E., McCallum, I., Robertson, E., Seufert, V., Fritz, S., Valade, A., Wiltshire, A., and Dolman, A. J.: Land management: data availability and process understanding for global change studies, *Glob Chang Biol*, 23, 512-533, 2017.

Foley, J. A., DeFries, R., Asner, G.P., Barford, C., Bonan, G., Carpenter, S.R., Chapin, F.S., Coe, M.T., Daily, G.C., Gibbs, H.K., Helkowski, J.H., Holloway, T., Howard, E.A., Kucharik, C.J., Monfreda, C., Patz, J.A., Colin Prentice, I., Ramankutty, N., Synder, P.K.: Global consequences of land use, *Science*, 309, 570-574, 2005.

Foley, J. A., Ramankutty, N., Brauman, K. A., Cassidy, E. S., Gerber, J. S., Johnston, M., Mueller, N. D., O'Connell, C., Ray, D. K., West, P. C., Balzer, C., Bennett, E. M., Carpenter, S. R., Hill, J., Monfreda, C., Polasky, S., Rockstrom, J., Sheehan, J., Siebert, S., Tilman, D., and Zaks, D. P.: Solutions for a cultivated planet, *Nature*, 478, 337-342, 2011.

Franklin, S. E., Ahmed, O. S., Wulder, M. A., White, J. C., Hermosilla, T., and Coops, N. C.: Large Area Mapping of Annual Land Cover Dynamics Using Multitemporal Change Detection and Classification of Landsat Time Series Data, *Canadian Journal of Remote Sensing*, 41, 293-314, 2015.

Friedl, M. A., Sulla-Menashe, D., Tan, B., Schneider, A., Ramankutty, N., Sibley, A., and Huang, X.: MODIS Collection 5 Global Land Cover: Algorithm Refinements and Characterization of New Datasets, *Remote Sensing of Environment*, 114, 168-182, 2010.

Gong, P., Li, X., Wang, J., Bai, Y., Chen, B., Hu, T., Liu, X., Xu, B., Yang, J., Zhang, W., and Zhou, Y.: Annual maps of global artificial impervious areas (GAIA) between 1985 and 2018, *Remote Sensing of Environment*, 236, 111510, 2020.

Gong, P., Liu, H., Zhang, M., Li, C., Wang, J., Huang, H., Clinton, N., Ji, L., Li, W., Bai, Y., Chen, B., Xu, B., Zhu, Z., Yuan, C., Ping Suen, H., Guo, J., Xu, N., Li, W., Zhao, Y., Yang, J., Yu, C., Wang, X., Fu, H., Yu, L., Dronova, I., Hui, F., Cheng, X., Shi, X., Xiao, F., Liu, Q., and Song, L.: Stable classification with limited sample: transferring a 30-m resolution sample set collected in 2015 to mapping 10-m resolution global land cover in 2017, *Science Bulletin*, 64, 370-373, 2019.

Hansen, M. C., Potapov, P.V., Moore, R., et al.: High-resolution global maps of 21st century forest cover change, *Science*, 342, 850-853, 2013.

Hermosilla, T., Wulder, M. A., White, J. C., Coops, N. C., and Hobart, G. W.: Disturbance-Informed Annual Land Cover Classification Maps of Canada's Forested Ecosystems for a 29-Year Landsat Time Series, *Canadian Journal of Remote Sensing*, 44, 67-87, 2018.

Homer, C., Dewitz, J., Jin, S., Xian, G., Costello, C., Danielson, P., Gass, L., Funk, M., Wickham, J., Stehman, S., Auch, R., and Riitters, K.: Conterminous United States land cover change patterns 2001–2016 from the 2016 National Land Cover Database, *ISPRS Journal of Photogrammetry and Remote Sensing*, 162, 184-199, 2020.



Jin, S., Yang, L., Danielson, P., Homer, C., Fry, J., and Xian, G.: A comprehensive change detection method for updating the National Land Cover Database to circa 2011, *Remote Sensing of Environment*, 132, 159-175, 2013.

Kennedy, R. E., Yang, Z., Braaten, J., Copass, C., Antonova, N., Jordan, C., and Nelson, P.: Attribution of disturbance change agent from Landsat time-series in support of habitat monitoring in the Puget Sound region, USA, *Remote Sensing of Environment*, 166, 271-285, 2015.

[LCMAP, LCMAP Collection 1 Science Products \[data\]. https://doi.org/10.5066/P9W1TO6E](https://doi.org/10.5066/P9W1TO6E), 2021.

[Li, X., Zhou, Y., Meng, L., Asrar, G. R., Lu, C., and Wu, Q.: A dataset of 30 m annual vegetation phenology indicators \(1985–2015\) in urban areas of the conterminous United States, \*Earth System Science Data\*, 11, 881-894, 2019.](#)

Li, X., Zhou, Y., Meng, L., Asrar, G. R., Lu, C., and Wu, Q.: A dataset of 30 m annual vegetation phenology indicators (1985–2015) in urban areas of the conterminous United States, *Earth System Science Data*, 11, 881-894, 2019.

Li, X., Zhou, Y., Zhu, Z., and Cao, W.: A national dataset of 30 m annual urban extent dynamics (1985–2015) in the conterminous United States, *Earth System Science Data*, 12, 357-371, 2020.

[NPS, 2021. Fire - Yellowstone National Park. https://www.nps.gov/yell/learn/nature/fire.htm#:~:text=Number%20in%20Yellowstone,human%20caused%20fires%20were%20suppressed.&text=The%20number%20of%20fires%20has.70%20C285%20acres%20in%20Yellowstone%20burned](https://www.nps.gov/yell/learn/nature/fire.htm#:~:text=Number%20in%20Yellowstone,human%20caused%20fires%20were%20suppressed.&text=The%20number%20of%20fires%20has.70%20C285%20acres%20in%20Yellowstone%20burned). Accessed in April 27, 2021.

Pengra, B. W., Stehman, S. V., Horton, J. A., and Wellington, D. F.: Land Change Monitoring, Assessment, and Projection (LCMAP) Version 1.0 Annual Land Cover and Land Cover Change Validation Tables, U.S. Geological Survey data release, [data], doi: <https://doi.org/10.5066/P98EC5XR>, 2020a.

Pengra, B. W., Stehman, S. V., Horton, J. A., Dockter, D. J., Schroeder, T. A., Yang, Z., and Loveland, T. R.: Quality control and assessment of interpreter consistency of annual land cover reference data in an operational national monitoring program, *Remote Sensing of Environment*, 238, 111261, 2020b.

Picotte, J. J., Dockter, D., Long, J., Tolck, B., Davidson, A., and Peterson, B.: LANDFIRE remap prototype mapping effort: Developing a new framework for mapping vegetation classification, change, and structure, *Fire*, 2, 35, 2019.

Reid, W. V., Chen, D., Goldfarb, L., Hackmann, H., Lee, Y. T., Mokehele, K., Ostrom, E., Raivio, K., Rockstrom, J., Schellhuber, H. J., and Whyte, A.: Earth System Science for Global Sustainability: Grand Challenges, *Science*, 330, 916-917, 2010.

Stehman, S. V., Pengra, B. W., Horton, J. A., and Wellington, D. F.: Validation of the U.S. Geological Survey's Land Change Monitoring, Assessment and Projection (LCMAP) Collection 1.0 annual land cover products 1985–2017, *Remote Sensing of Environment*, 265, 2021.

Szantoi, Z., Geller, G. N., Tsendbazar, N.-E., See, L., Griffiths, P., Fritz, S., Gong, P., Herold, M., Mora, B., and Obregón, A.: Addressing the need for improved land cover map products for policy support, *Environmental Science & Policy*, 112, 28-35, 2020.

Tibshirani, R.: Regression shrinkage and selection via the lasso, *Journal of the Royal Statistical Society: Series B (Methodological)*, 58, 267-288, 1996.

Turner II, B. L., Lambin, E. F., and Reeberg, A.: The emergence of land change science for global environmental change and sustainability, *Proceedings of the National Academy of Sciences of the United States of America*, 104, 20666-20671, 2007.

Field Code Changed

Underwood, E. C., Ustin, S. L., and Ramirez, C. M.: A comparison of spatial and spectral image resolution for mapping invasive plants in coastal California, *Environ Manage*, 39, 63-83, 2007.

Wickham, J. D., Stehman, S. V., Fry, J. A., Smith, J. H., and Homer, C. G.: Thematic accuracy of the NLCD 2001 land cover for the conterminous United States, *Remote Sensing of Environment*, 114, 1286-1296, 2010.

Wulder, M. A., Coops, N. C., Roy, D. P., White, J. C., and Hermosilla, T.: Land cover 2.0, *International Journal of Remote Sensing*, 39, 4254-4284, 2018.

Xian, G., Homer, C., Meyer, D., and Granneman, B.: An approach for characterizing the distribution of shrubland ecosystem components as continuous fields as part of NLCD, *ISPRS Journal of Photogrammetry and Remote Sensing*, 86, 136-149, 2013.

Zhou, Q., Tollerud, H. J., Barber, C. P., Smith, K., and Zelenak, D.: Training data selection for annual land cover classification for the land change monitoring, assessment, and projection (LCMAP) initiative, *Remote Sensing*, 12, 699, 2020.

Zhu, Z., Gallant, A. L., Woodcock, C. E., Pengra, B., Olofsson, P., Loveland, T. R., Jin, S., Dahal, D., Yang, L., and R.F., a. A.: Optimizing selection of training and auxiliary data for operational land cover classification for the LCMAP initiative, *ISPRS Journal of Photogrammetry and Remote Sensing* 122, 206-221, 2016.

Zhu, Z., Wang, S., and Woodcock, C. E.: Improvement and expansion of the Fmask algorithm: Cloud, cloud shadow, and snow detection for Landsats 4–7, 8, and Sentinel 2 images, *Remote Sensing of Environment*, 159, 269-277, 2015a.

Zhu, Z. and Woodcock, C. E.: Automated cloud, cloud shadow, and snow detection in multitemporal Landsat data: An algorithm designed specifically for monitoring land cover change, *Remote Sensing of Environment*, 152, 217-234, 2014a.

Zhu, Z. and Woodcock, C. E.: Continuous change detection and classification of land cover using all available Landsat data, *Remote Sensing of Environment*, 144, 152-171, 2014b.

Zhu, Z. and Woodcock, C. E.: Object-based cloud and cloud shadow detection in Landsat imagery, *Remote Sensing of Environment*, 118, 83-94, 2012.

Zhu, Z., Woodcock, C. E., Holden, C., and Yang, Z.: Generating synthetic Landsat images based on all available Landsat data: Predicting Landsat surface reflectance at any given time. , *Remote Sensing of Environment*, 162, 67-83, 2015b.

### Caption of Table

Table 1 LCMAP land cover product specifications

Table 2 NLCD land cover cross-walked to LCMAP land cover

Table 3. Confusion matrix for CONUS (all years combined) where cell entries represent percent of CONUS area. Overall accuracy is 82.5% ( $\pm 0.22\%$ ). Standard errors for user's and producer's accuracies are shown in parentheses and  $n$  is the number of sample pixels for each row and column.

Table 4 Overall per class agreement in percentage between 1985 and 2017

### Caption of Figure

Figure 1 Landsat ARD tile grids for the conterminous U.S.

Figure 2 Overall procedures of the CCD algorithm.

[Figure 3 The overall approach of land cover classification in CCDC.](#)

Figure ~~43~~. ~~Figure 3~~—NLCD 2001 land cover (a), cross-walked LCMAP land cover classes (b), LCMAP land cover eroded by one pixel (c), zoomed in cross-walked land cover from NLCD 2001 (d), and zoomed in LCMAP land cover classes eroded by one pixel (e). The color legends represent NLCD land cover class and LCMAP primary land cover (LCPRI).

Figure ~~54~~ CCD change detection and segmentation using Landsat blue, green, red, near-infrared, short-wave infrared (SWIR) 1, short-wave infrared (SWIR) 2, and thermal bands. Blue dots are all available clear Landsat records in each year. The horizontal lines in different colors represent land cover classes labeled by the algorithm. The vertical lines show model break dates. The back line is the model fits. The high-resolution images show landscape conditions in 2007 and 2013.

Figure ~~56~~ Illustration of the LCMAP product: (a) Primary land cover in 2010, (b) Primary land cover confidence in 2010, (c) ~~the frequency total number~~ of land cover changes from 1985 to 2017, and (d) total number of ~~spectral~~ changes detected from 1985 to 2017.

Figure ~~76~~ Areal variations of eight primary land cover types from 1985 to 2017 in CONUS.

Figure ~~87~~ Primary land cover and confidences in 1985 (a) and (d), 1990 (b) and (e), 2016(c) and (f), change in 1985-2017 (g), [the frequency of land cover change \(x-axis\) from 1985 to 2017 and](#)

[numbers of total pixels \(y-axis\) of these changes of different change \(h\), and areas \(y-axis\) of different land cover \(x-axis\) total pixels of different change \(h\), and areas of different land cover](#) in the three times for the ARD tile 16\_14 (i).

Figure [89](#) Primary land cover and confidences in 1985 (a) and (d), 1990 (b) and (e), 2016 (c) and (f), and change in 1985-2017 (g), [the frequency of land cover change \(x-axis\) from 1985 to 2017 and numbers of pixels \(y-axis\) of these changes \(h\), and areas \(y-axis\) of different land cover \(x-axis\) total pixels of different change \(h\), and areas of different land cover](#) in the three times for the ARD tile 9\_6 (i).

Figure [109](#) Overall agreement between LCMAP primary land cover and reference data across CONUS. The cross lines represent +/- one standard errors.

Table 1 LCMAP land cover product specifications

Code	Land Cover Class	Description
1	<b>Developed</b>	Areas of intensive use with much of the land covered with structures (e.g., high-density residential, commercial, industrial, mining, or transportation), or less intensive uses where the land cover matrix includes vegetation, bare ground, and structures (e.g., low-density residential, recreational facilities, cemeteries, transportation/utility corridors, etc.), including any land functionality related to the developed or built-up activity.
2	<b>Cropland</b>	Land in either a vegetated or unvegetated state used in production of food, fiber, and fuels. This includes cultivated and uncultivated croplands, hay lands, orchards, vineyards, and confined livestock operations. Forest plantations are considered as forests or woodlands (Tree Cover class) regardless of the use of the wood products.
3	<b>Grass/Shrub</b>	Land predominantly covered with shrubs and perennial or annual natural and domesticated grasses (e.g. pasture), forbs, or other forms of herbaceous vegetation. The grass and shrub cover must comprise at least 10% of the area and tree cover is less than 10% of the area.
4	<b>Tree Cover</b>	Tree-covered land where the tree cover density is greater than 10%. Cleared or harvested trees (i.e. clearcuts) will be mapped according to current cover (e.g. Barren, Grass/Shrub).

5	<b>Water Bodies</b>	Areas covered with water, such as streams, canals, lakes, reservoirs, bays, or oceans.
6	<b>Wetland</b>	Lands where water saturation is the determining factor in soil characteristics, vegetation types, and animal communities. Wetlands are composed of mosaics of water, bare soil, and herbaceous or wooded vegetated cover.
7	<b>Ice and Snow</b>	Land where accumulated snow and ice does not completely melt during the summer period (i.e. perennial ice/snow).
8	<b>Barren</b>	Land comprised of natural occurrences of soils, sand, or rocks where less than 10% of the area is vegetated.

Table 2 NLCD land cover cross-walked to LCMAP land cover

<b>NLCD Value</b>	<b>LCMAP Value</b>
Water	Water
Ice/Snow	Ice and Snow
Developed, open space; Developed, low intensity; Developed medium intensity; Developed, high intensity	Developed
Barren	Barren
Deciduous forest, Evergreen forest, Mixed forest	Tree Cover
Shrub/Scrub, Grassland/Herbaceous	Grass/Shrub
Hay/Pasture, Cultivated crops	Cropland
Woody wetland, Emergent herbaceous wetland	Wetland

Table 3. Confusion matrix for CONUS (all years combined) where cell entries represent percent of CONUS area. Overall accuracy is 82.5% ( $\pm 0.22\%$ ). Standard errors for user's and producer's accuracies are shown in parentheses and  $n$  is the number of sample pixels for each row and column.

Map	Devel	Crop.	Grass /Shrub	Tree	Water	Wetland	Ice/Snow	Barren	Total	User (SE)	$n$
Devel.	<b>3.000</b>	0.139	0.321	0.377	0.024	0.035		0.001	3.896	77 (1.2)	32102
Crop.	0.918	<b>16.527</b>	5.061	0.799	0.027	0.368		0.003	23.702	70 (0.6)	195283
Grass /Shrub	0.368	0.757	<b>30.649</b>	2.599	0.045	0.229		0.332	34.980	88 (0.3)	288197
Tree	0.340	0.143	1.414	<b>23.387</b>	0.049	0.579		0.006	25.917	90 (0.3)	213531
Water	0.013	0.008	0.048	0.024	<b>4.788</b>	0.067		0.020	4.968	96 (0.5)	40932
Wetland	0.062	0.129	0.361	0.944	0.172	<b>3.688</b>		0.001	5.357	69 (1.3)	44136
Ice/Snow			0.004	0.004		0.004	<b>0.012</b>	0.004	0.028	43 (18.7)	231
Barren	0.072	0.005	0.501	0.013	0.056	0.012		<b>0.492</b>	1.151	43 (2.8)	9485
Total	4.772	17.707	38.358	28.149	5.162	4.981	0.012	0.859	100.00		
Prod (SE)	63 (1.3)	93 (0.3)	80 (0.4)	83 (0.4)	93 (0.7)	74 (1.2)	100 (0)	57 (3.2)			
$n$	39319	145886	316027	231916	42530	41042	99	7078			

Table 4 Overall per class agreement in percentage between 1985 and 2017

Overall Per Class Agreement	Developed	Cropland	Grass/Shrub	Tree	Water	Wetland	Snow/Ice	Barren
1985	66	80	83	87	95	72	60	49
1986	67	80	83	87	95	72	60	49
1987	68	80	83	86	95	72	60	49
1988	68	80	83	87	95	72	60	49
1989	68	80	84	87	95	72	60	48
1990	68	80	84	87	95	72	60	48
1991	68	80	84	87	95	72	60	49
1992	69	80	84	87	95	71	60	50
1993	69	80	84	87	95	71	60	49
1994	69	80	84	87	95	71	60	49
1995	70	80	84	87	95	72	60	49
1996	69	80	84	87	95	72	60	48
1997	70	80	84	87	95	72	60	49
1998	70	80	84	87	94	72	60	48
1999	70	80	84	87	95	72	60	48
2000	70	80	84	87	95	72	60	48
2001	70	80	84	87	95	72	60	49
2002	70	80	84	86	95	72	60	49
2003	70	80	84	87	94	71	60	48
2004	69	80	84	86	94	71	60	48
2005	70	80	84	86	94	71	60	49
2006	70	79	84	86	94	71	60	49
2007	70	79	84	86	94	71	60	50
2008	70	79	84	86	94	71	60	49
2009	70	79	84	86	94	71	60	49
2010	70	79	84	86	94	71	60	50
2011	70	79	84	86	94	71	60	51
2012	70	79	83	86	94	71	60	50
2013	69	79	83	86	94	71	60	50
2014	69	79	83	86	94	71	60	50
2015	69	79	83	86	94	71	60	50
2016	69	79	83	86	94	71	60	50
2017	69	78	83	85	94	70	60	49

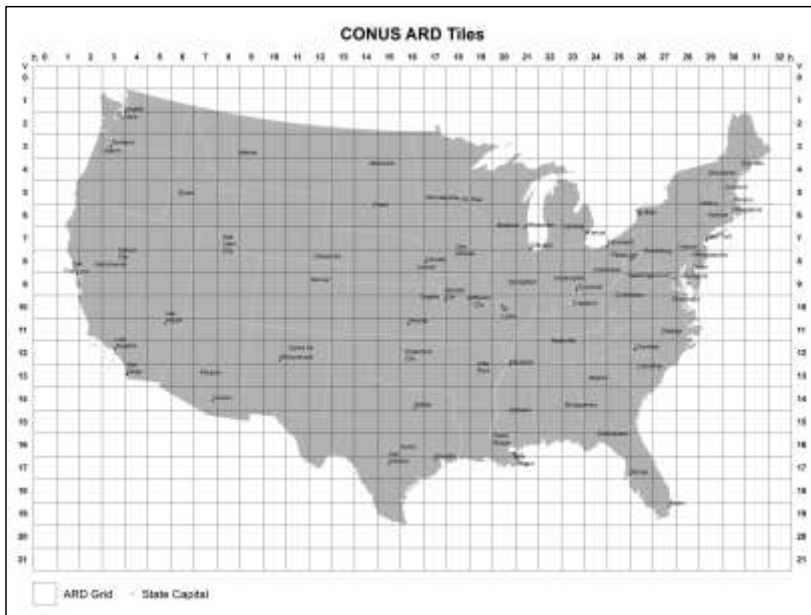


Figure 1 Landsat ARD tile grids for the conterminous U.S.



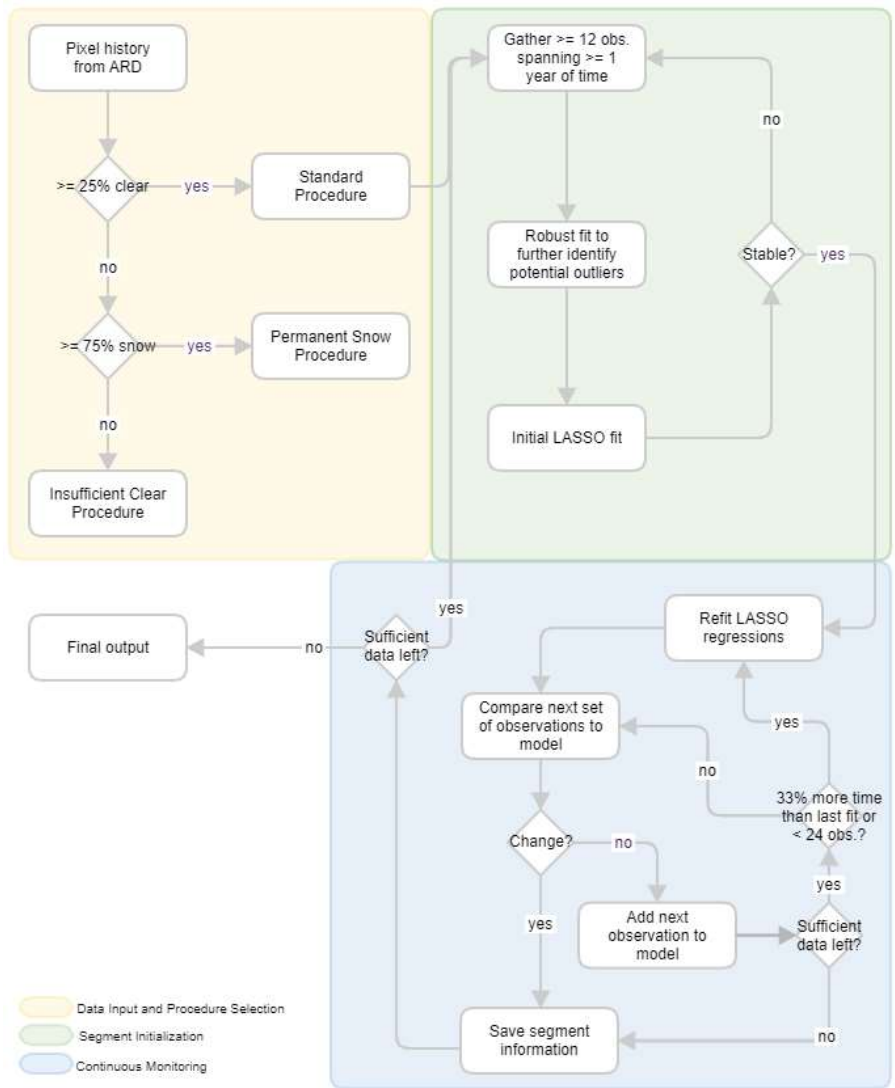


Figure 2 Overall procedures of the CCD algorithm.

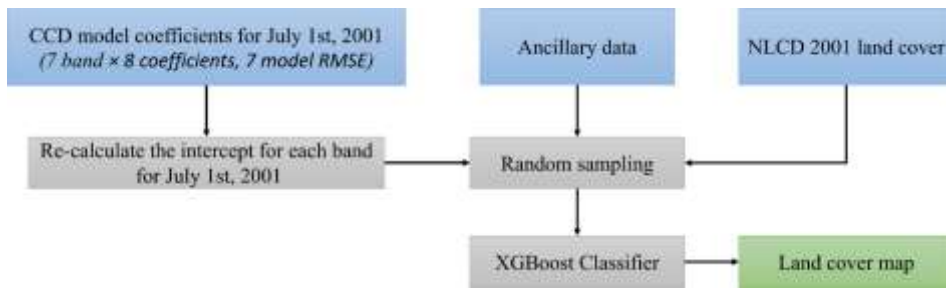


Figure 3 The overall approach of land cover classification in CCDC.

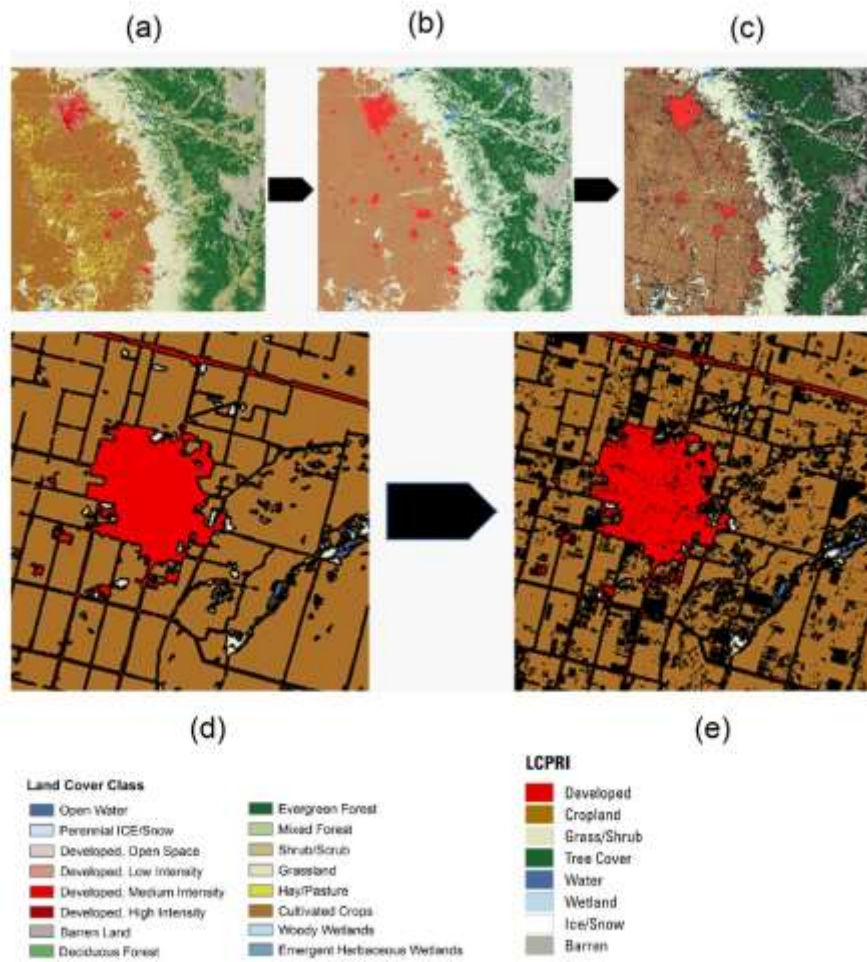


Figure 43. NLCD 2001 land cover (a), cross-walked LCMAP land cover classes (b), LCMAP land cover eroded by one pixel (c), zoomed in cross-walked land cover from NLCD 2001 (d), and zoomed in LCMAP land cover classes eroded by one pixel (e). The color legends represent NLCD land cover class and LCMAP primary land cover (LCPRI).

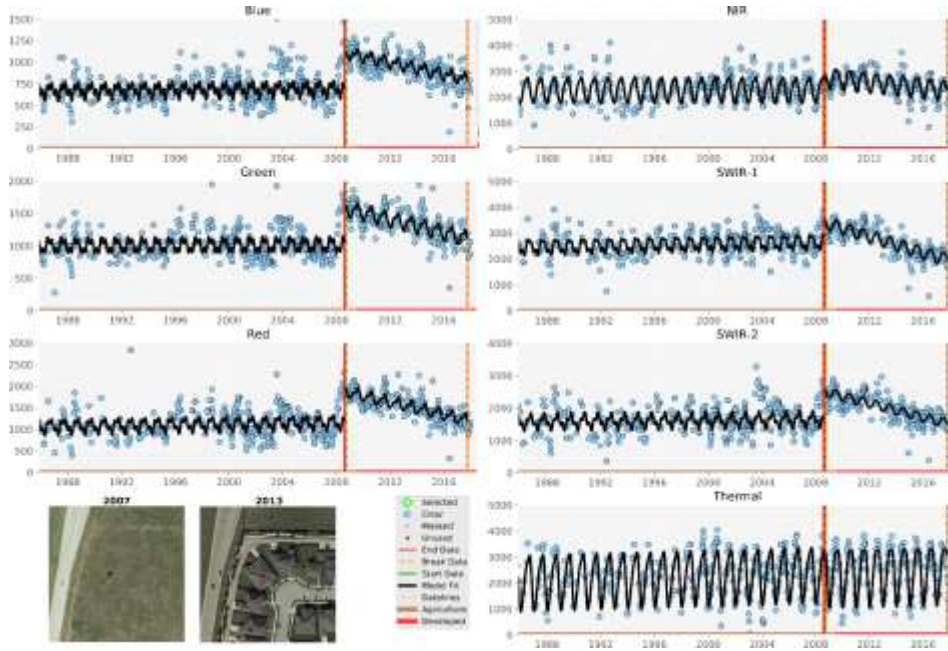
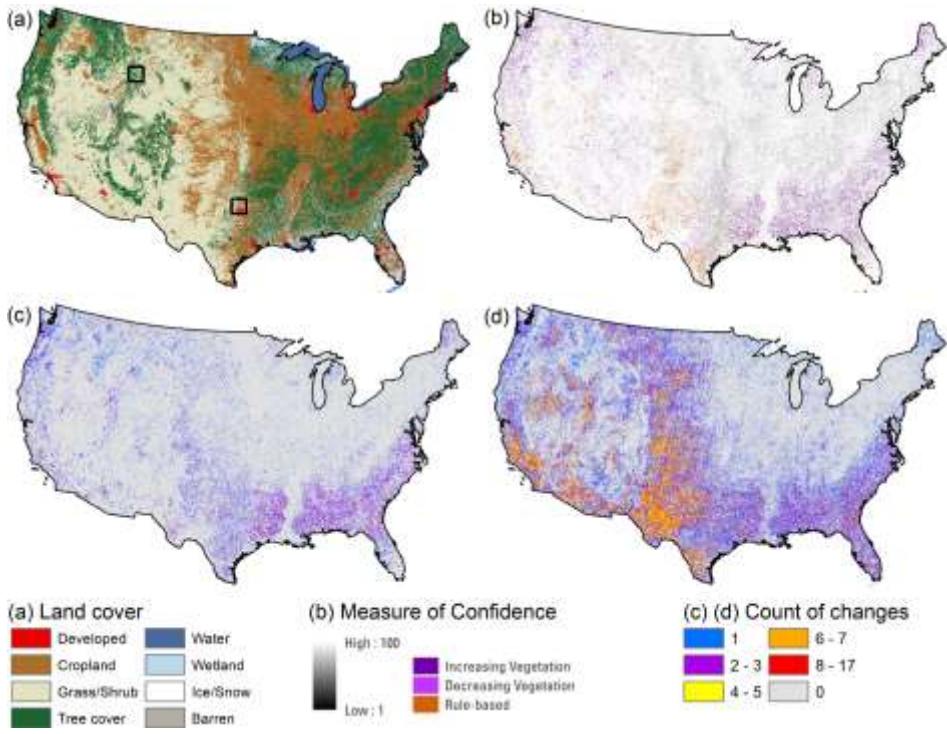


Figure 45 CCD change detection and segmentation using Landsat blue, green, red, near-infrared, short-wave infrared (SWIR) 1, short-wave infrared (SWIR) 2, and thermal bands. Blue dots are all available clear Landsat records in each year. The horizontal lines in different colors represent land cover classes labeled by the algorithm. The vertical lines show model break dates. The black line is the model fits. The high-resolution images show landscape conditions in 2007 and 2013.



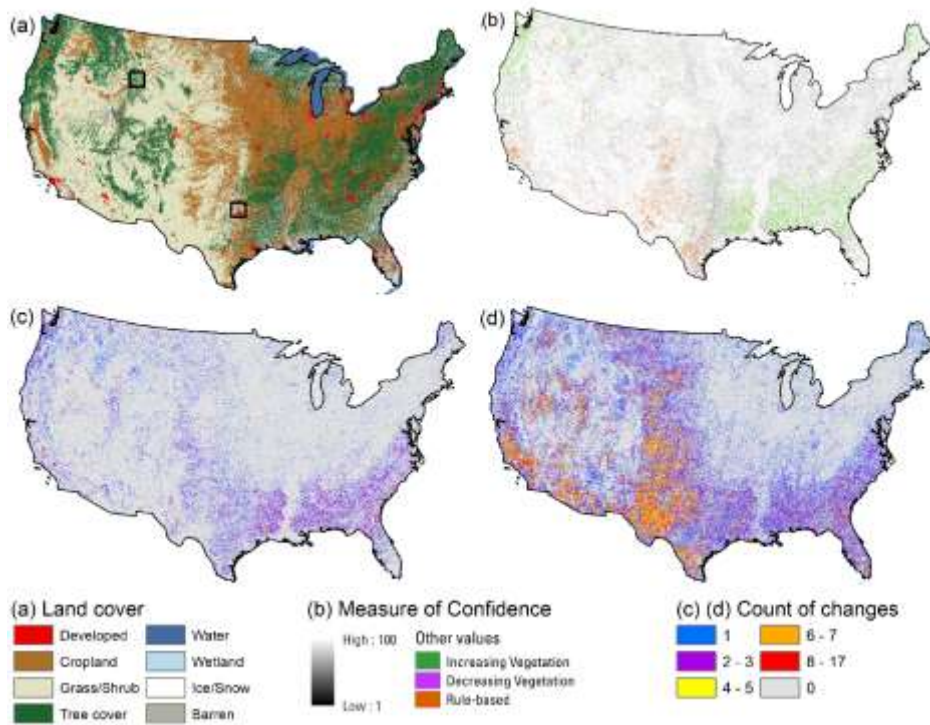


Figure 65 Illustration of the LCMAP product: (a) Primary land cover in 2010, (b) Primary land cover confidence in 2010, (c) the frequency total number of land cover changes from 1985 to 2017, and (d) total number of spectral changes detected from 1985 to 2017.

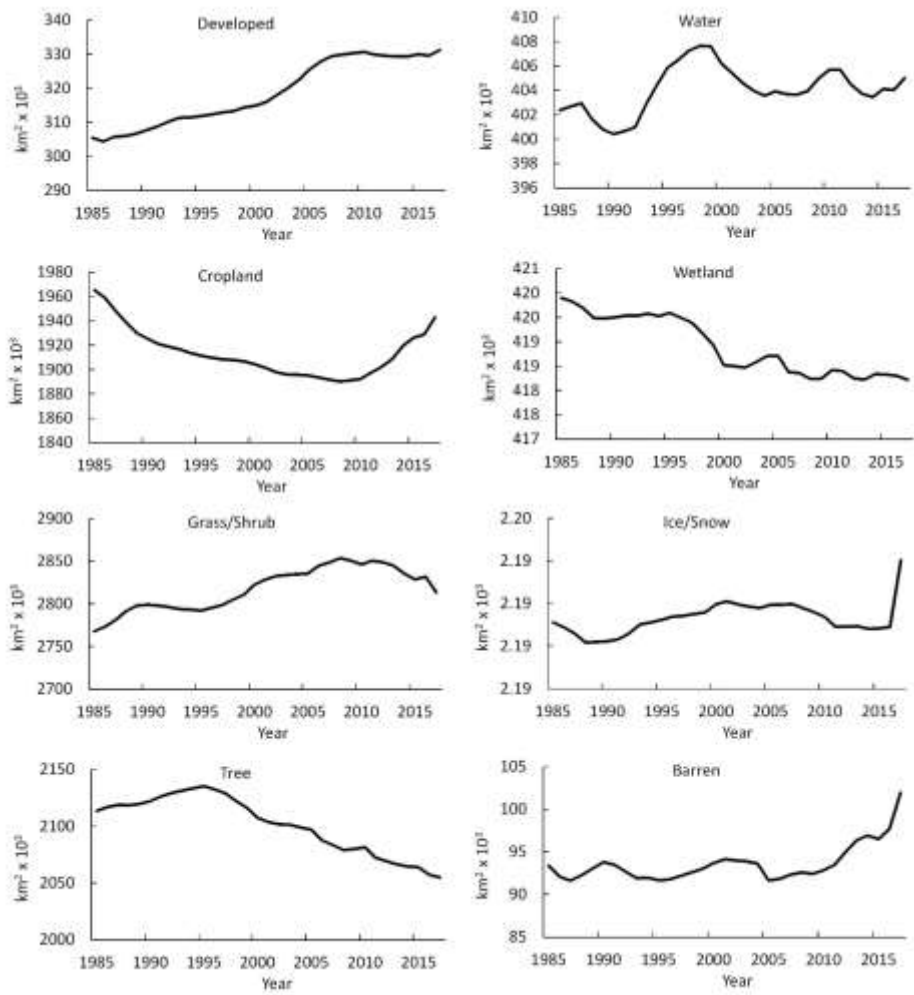
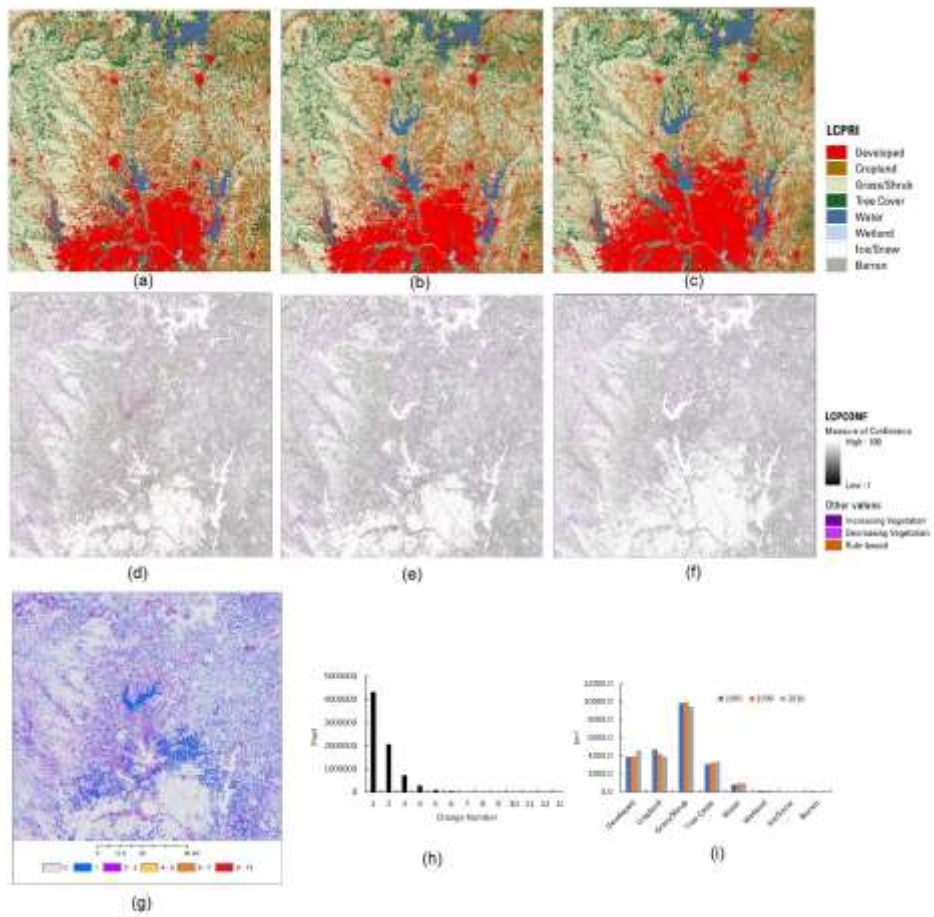


Figure 76 Areal variations of eight primary land cover types from 1985 to 2017 in CONUS.





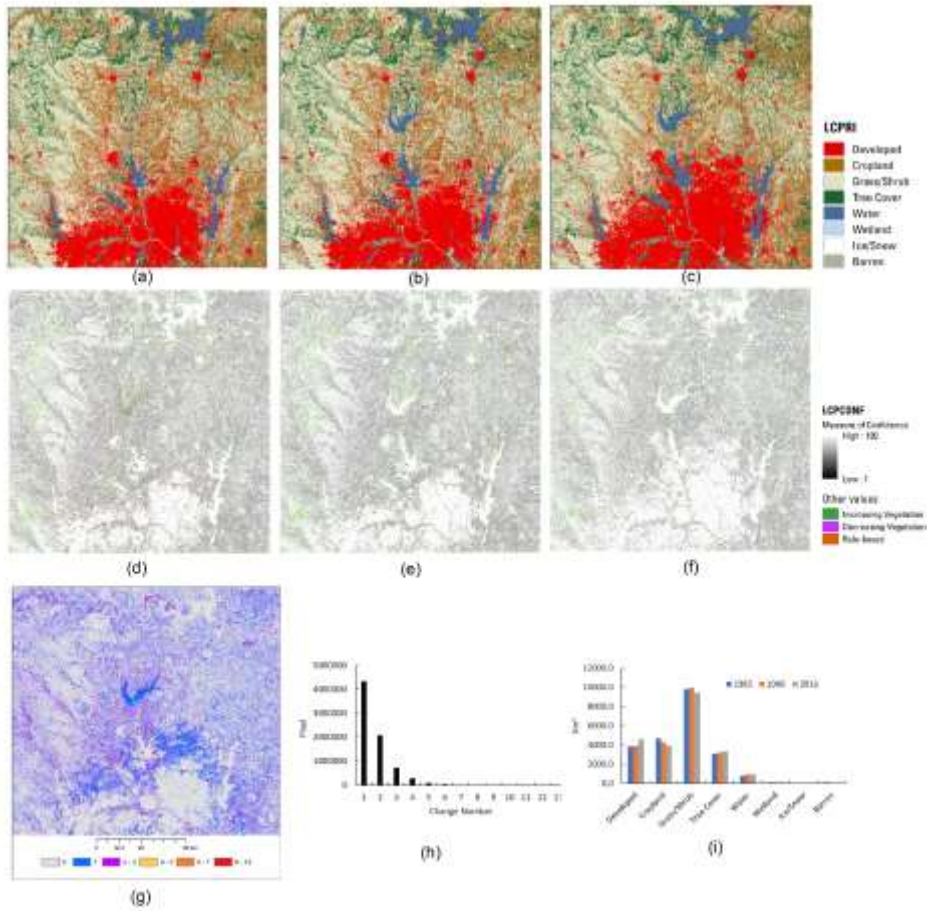
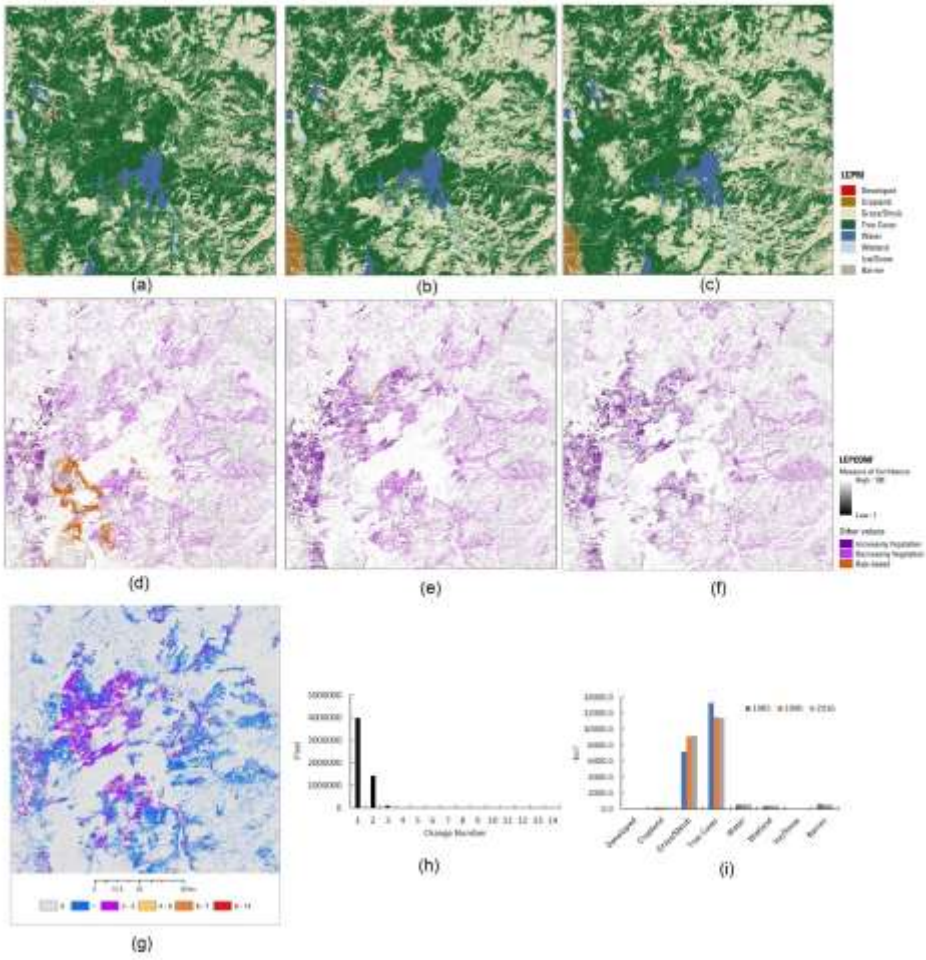


Figure 87 Primary land cover and confidences in 1985 (a) and (d), 1990 (b) and (e), 2016(c) and (f), change in 1985-2017 (g), the frequency of land cover change (x-axis) from 1985 to 2017 and numbers of total pixels (y-axis) of these changes of different change (h), and areas (y-axis) of different land cover (x-axis) in the three times for the ARD tile 16\_14 (i).



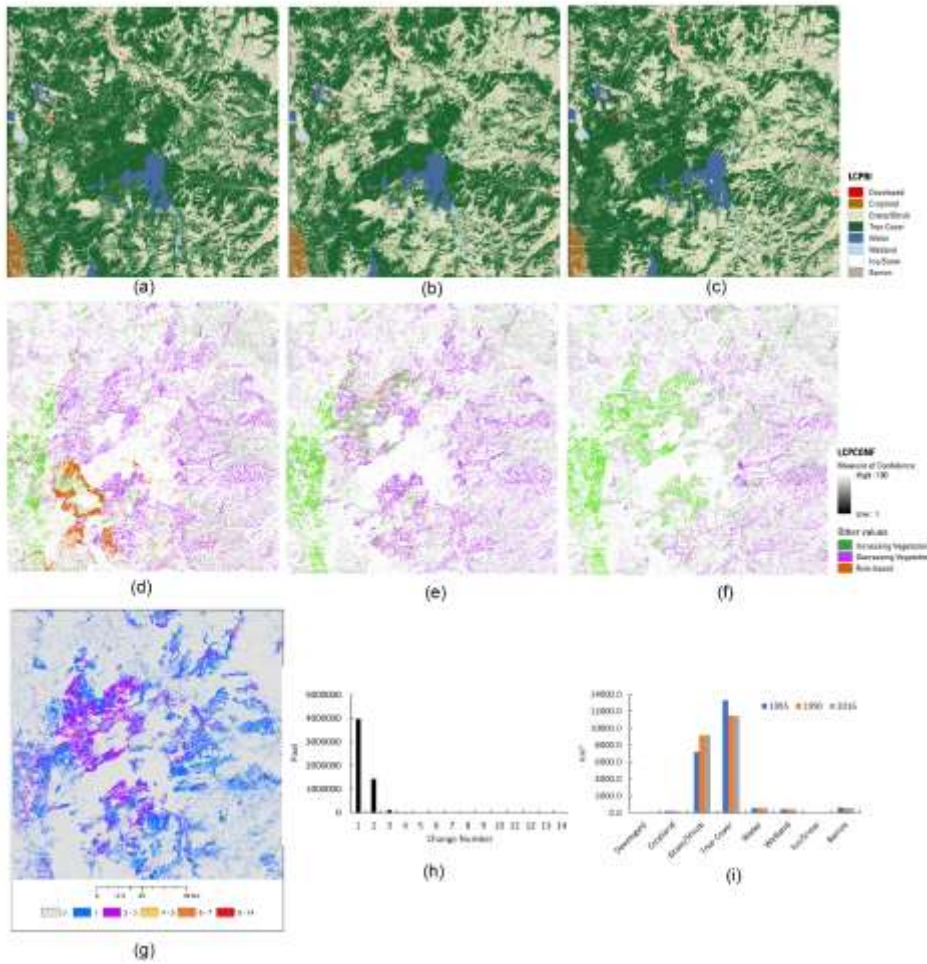


Figure 89 Primary land cover and confidences in 1985 (a) and (d), 1990 (b) and (e), 2016 (c) and (f), and change in 1985-2017 (g), -the frequency of land cover change (x-axis) from 1985 to 2017 and numbers of pixels (y-axis) of these changes (h), total pixels of different change (h), and areas of different land cover and areas (y-axis) of different land cover (x-axis)-in the three times for the ARD tile 9\_6 (i).

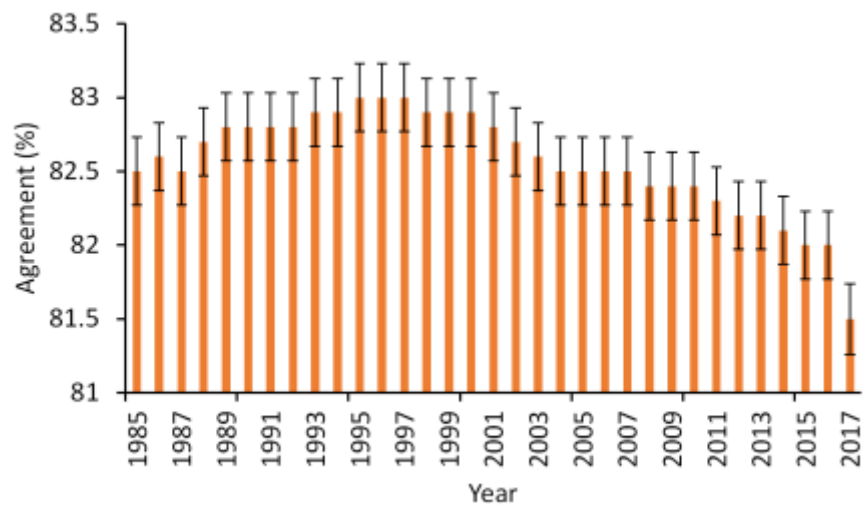


Figure 109 Overall agreement between LCMAP primary land cover and reference data across CONUS. The cross lines represent +/- one standard errors.